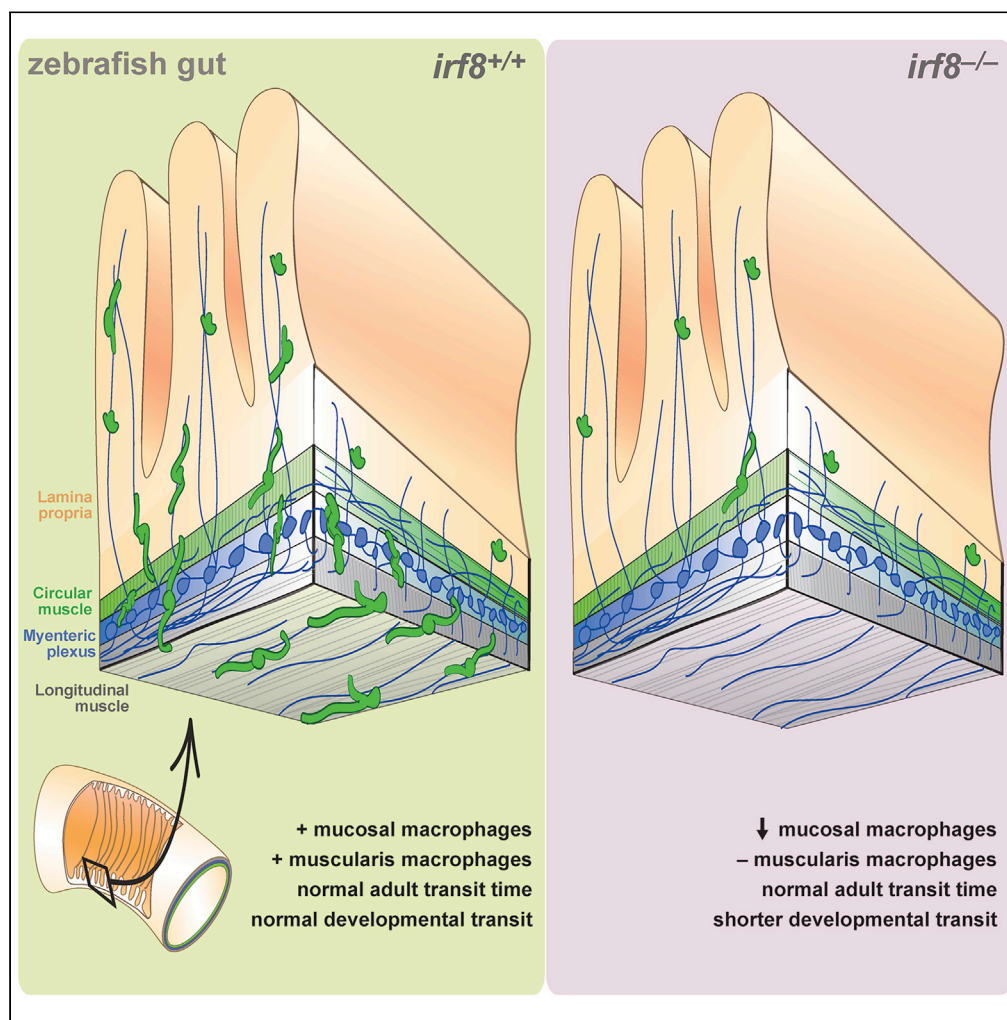


Article

Zebrafish harbor diverse intestinal macrophage populations including a subset intimately associated with enteric neural processes



Christina L. Graves, Angela Chen, Victoria Kwon, Celia E. Shiau

shiauce@unc.edu

Highlights

Zebrafish harbor intestinal muscularis and mucosal macrophages similar to mammals

Muscularis and mucosal macrophages closely associate with enteric neural processes

Individual muscularis macrophages span several gut layers in zebrafish

Selective muscularis macrophage elimination by *irf8* ablation affects intestinal transit

Graves et al., iScience 24, 102496
June 25, 2021 © 2021 The Author(s).
<https://doi.org/10.1016/j.isci.2021.102496>



Article

Zebrafish harbor diverse intestinal macrophage populations including a subset intimately associated with enteric neural processes

Christina L. Graves,^{1,3} Angela Chen,¹ Victoria Kwon,¹ and Celia E. Shiau^{1,2,4,*}

SUMMARY

Intestinal macrophages are essential for gut health but remain understudied outside of human and mouse systems. Here, we establish zebrafish as a powerful model that provides superior imaging capabilities for whole-gut analysis along all dimensions (anterior-posterior and center-outer axes) for dissecting macrophage biology in gastrointestinal health and disease. We utilized high-resolution imaging to show that the zebrafish gut contains *bona fide* muscularis and mucosal macrophages, as well as surprisingly large subsets intimately associated with enteric neural processes. Interestingly, most muscularis macrophages span multiple gut layers in stark contrast to their mammalian counterparts typically restricted to a single layer. Using macrophage-deficient *irf8* zebrafish, we found a depletion of muscularis but not mucosal macrophages, and that they may be dispensable for gross intestinal transit in adults but not during development. These characterizations provide first insights into intestinal macrophages and their association with the enteric nervous system from development to adulthood in teleosts.

INTRODUCTION

Macrophages adapt to tissue-specific niches

Élie Metchnikoff's descriptions of phagocytic cells more than 100 years ago heralded a new era of immunology rooted largely in the innate recognition and responses of these highly mobile sentinels. Growing evidence demonstrating the function of macrophages (m ϕ) in antigen processing, presentation and coordination of adaptive immunity (Elhelu, 1983) has strengthened the immune-centric view of these cells. M ϕ densely inhabit most tissues highlighting their ubiquitous importance in maintaining cellular and organismal homeostasis (Lavin and Merad, 2013; Lavin et al., 2015). More recently studies are increasingly establishing the physical association of m ϕ within different tissues leading to characterization of their role in homeostatic tissue development, maintenance, remodeling, inflammation, and regeneration (Okabe and Medzhitov, 2016; Yang et al., 2020; Shiau et al., 2013). Rather than being disparate, these complementary functions of m ϕ appear to reflect their nature as an ontologically and functionally diverse, heterogeneous, highly plastic cell type (Morales and Allende, 2019; Ginhoux and Guilliams, 2016).

Once thought to be exclusively derived from circulating monocytes (Cohn, 1968), it is now widely accepted that early developmentally seeded, long-lived resident m ϕ pool exists in most tissues (Davies et al., 2013; Epelman et al., 2014). These resident m ϕ appear to be adapted to the local tissue microenvironment and uniquely positioned to rapidly respond to tissue insult (Okabe and Medzhitov, 2016) although their complete developmental origin and capacity for self-renewal remain incompletely understood (Jutila and Banks, 1986; De Schepper et al., 2018). Evidence supporting a tissue-specific niche and function derives from studies on microglia, brain-resident m ϕ (Davies et al., 2013), which are among the best characterized with regards to their tissue specificity. In addition to serving as a 'first line of defense,' microglia play roles in cellular scavenging, synapse pruning, neuronal survival, circuitry remapping post damage and have the capacity to undergo rapid phenotypic transformation in response to local conditions (Sawada, 1999; Paolicelli et al., 2011; Harry, 2013; Rubino et al., 2018). Other studies have described resident m ϕ populations adapted to the unique needs of host tissues, including that of skin (Langerhans cells) (Doebel et al., 2017; Gomez Perdiguero et al., 2015), liver (Kupffer cells) (Krenkel and Tacke, 2017; Bilzer et al., 2006; Dixon et al., 2013), lung (alveolar m ϕ) and gut (Wehner et al., 2007; Earley et al., 2018b; Shaw et al., 2018; Matheis et al., 2020)

¹Department of Biology, University of North Carolina Chapel Hill, Chapel Hill, NC 27599, USA

²Department of Microbiology and Immunology, University of North Carolina Chapel Hill, Chapel Hill, NC 27599, USA

³Present address: Adams School of Dentistry, University of North Carolina Chapel Hill, Chapel Hill, North Carolina, 27599 USA

⁴Lead contact

*Correspondence: shiauce@unc.edu

<https://doi.org/10.1016/j.isci.2021.102496>



but detailed mechanistic and comprehensive understanding of their function in development, health and disease remains to be achieved.

Mammalian gut macrophages are anatomically and functionally heterogeneous

Increasing interest in the function and origin of gut-residing m ϕ have yielded insight into gut m ϕ diversity in mammals (Bujko et al., 2018; Shaw et al., 2018), where gut m ϕ are known to comprise a functionally, morphologically, and ontologically diverse population [for a recent review of gut m ϕ (Muller et al., 2020)]. At steady-state, gut m ϕ occupy all regions (small intestine, stomach, large intestine, and colon) and all layers of the gut wall (mucosal, submucosal, and muscular); they also appear functionally specialized to each niche (Gabanyi et al., 2016; Chieppa et al., 2006). Most gut m ϕ research has focused on the mucosal population. Mucosal macrophages which are epithelium-associated m ϕ nearest the gut lumen appear to perform specialized functions in scavenging and phagocytosing potential pathogens and apoptotic epithelial cells (Wehner et al., 2007; De Schepper et al., 2018). In the underlying lamina propria (an immune-rich compartment underlying the gut epithelium), m ϕ skew local immune responses through antigen presentation and cytokine production (Mcdole et al., 2012; Schenk and Mueller, 2007). An anatomically distinct gut m ϕ pool is also found in the intestinal muscularis (muscularis externa) which is densely innervated by nerves and appears to be otherwise immune cell-poor (Gabanyi et al., 2016), which are referred to as muscularis macrophages (MM ϕ).

These MM ϕ have been described in humans and other mammalian organisms including mouse, cat, guinea pig, rabbit, as well as in non-mammalian organisms such as the chicken suggesting they are evolutionarily conserved across vertebrates (Mikkelsen, 1995, 2010). MM ϕ are identifiable in part by their stereotypical maximum-distance patterning (similar to other tissue-resident m ϕ) and by their intimate apposition to enteric-associated neurons and processes (Gabanyi et al., 2016). Given that they are also anatomically associated with interstitial cells of Cajal (the peristaltic ‘pacemakers’ of the gut), it is perhaps unsurprising that MM ϕ have been implicated to regulate gut peristalsis and motility (Mikkelsen, 2010; Muller et al., 2020). Recent studies in mice have described MM ϕ beta-2-adrenergic receptor (β 2-AR) functions, including the ability to limit infection-associated enteric neuronal loss (Matheis et al., 2020). MM ϕ have also been implicated in several diseases where intestinal motility is strikingly impaired including type 1 diabetes and gastroparesis (Choi et al., 2010). Taken together, these studies provide foundational work in mammalian systems implicating motility-oriented and neuroprotective roles for gut MM ϕ .

Zebrafish are an emerging model to study mucosal immunology and neuroimmune interactions

Zebrafish (*Danio rerio*) is a powerful model system due to its genetic tractability, fecundity, and optical transparency during embryonic and early larval stages (Darrow and Harris, 2004; Renshaw and Trede, 2012; Goldsmith and Jobin, 2012; Earley et al., 2018a). More recently, zebrafish have emerged as a highly tractable model organism for interrogating steady-state intestinal physiology and disease (Flores et al., 2020; Zhao and Pack, 2017; Lu et al., 2017). The strengths of zebrafish also allow for direct interrogation of innate-immune centric neuroimmune interactions during development and surveillance of the entire gut length; the thin nature of the gut tissue relative to larger mammals such as mice also allows for an increased imaging depth into the gut.

Our recent work in zebrafish describes a critical role of gut macrophages in shaping the intestinal microbiota (Earley et al., 2018b). We uncovered a conditional requirement for *interferon regulatory factor-8* (*irf-8*) in the development and maintenance of zebrafish macrophages including those of the gut. Although we have characterized some aspects of zebrafish intestinal m ϕ development and function, whether zebrafish contains the full breadth of anatomical m ϕ diversity (more completely described in mammalian systems) has been hereto unexplored (Earley et al., 2018b). Given that zebrafish have been a powerful model system for understanding the pathophysiology of a variety of human-relevant diseases and uncovering basic cellular principles, we expect advances in understanding gut macrophage diversity in zebrafish, such as those described here, will significantly advance our understanding in mucosal immunology, gut health, and neuroimmune interactions (Yang et al., 2020; Earley et al., 2018b; Zhao and Pack, 2017; Brugman, 2016; Lickwar et al., 2017). Specifically, determining the extent of morphological and anatomical heterogeneity of gut m ϕ provides crucial insights toward an improved understanding of the role of innate immunity in gastrointestinal homeostasis and health. Our study establishes zebrafish as a model organism

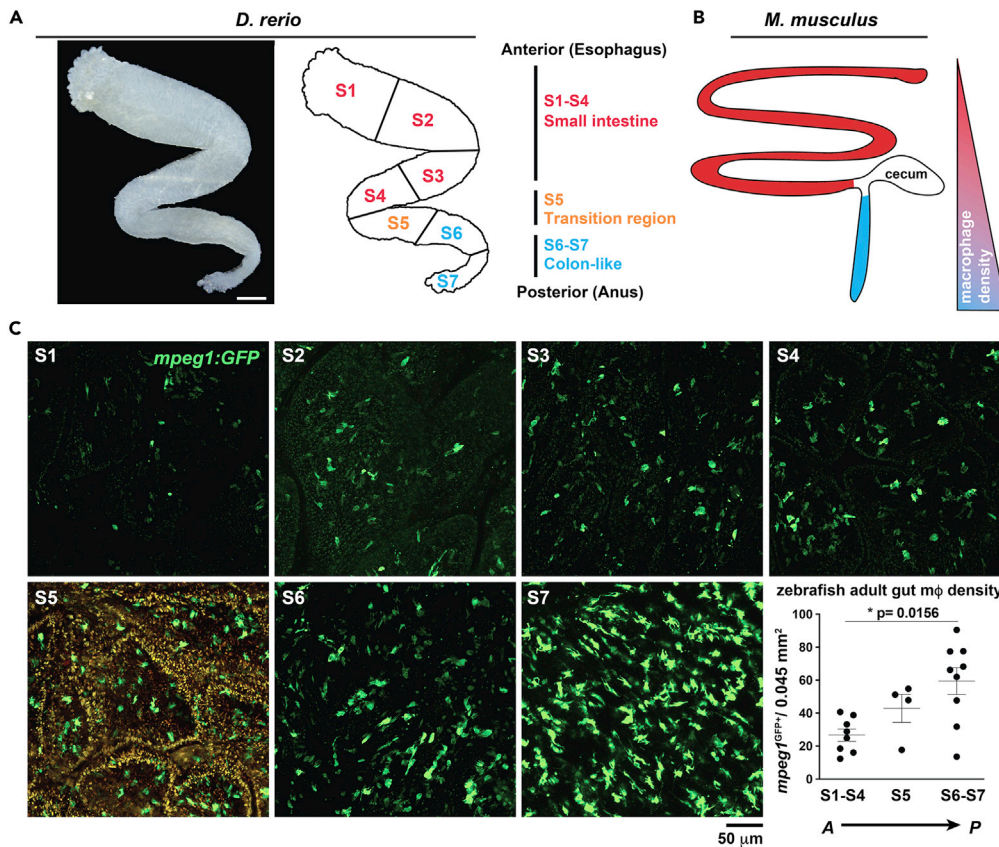


Figure 1. Increased macrophage density in the posterior (distal) gut of adult zebrafish

(A) (A, left) Transmitted light micrograph shows ex vivo dissected zebrafish adult gut tube (scale 500 μm). (A, right) Anterior to posterior organization highlighting small intestine-like (S1-S4, red), transition (S5, orange) and large-intestine like (S6-S7, blue) anatomical regions.

(B) (B, left) Anterior to posterior organization of adult mouse gut showing corresponding small (red) and large intestinal (blue) regions and (B, right) corresponding relative mφ density.

(C) Representative confocal micrographs of adult Tg(*mpeg1:GFP*) ex vivo whole-mount dissected gut opened longitudinally and imaged from the luminal side at indicated regions (S1 - S7) and corresponding mφ density of each gut region (graph). Region S5 is shown with both FITC and TRITC channels overlaid to enhance visualization of *mpeg1*^{GFP+} signal over high S5-region tissue autofluorescence (orange signal). Micrograph data are representative of >20 samples of >4 independent experiments. Data shown reflect the average of 2 independent regions per n = 8–9 (S1-4 and S6-7) or n = 4 (S5) of experimental individuals. Significance of *p = 0.0156 determined by one-way non-parametric ANOVA (Kruskal-Wallis). Scale bars are shown as indicated.

for interrogating these questions and provides the groundwork for further exploration of the diversity and function of macrophages in normal and diseased gut physiology.

RESULTS

Increased mφ density in the distal adult zebrafish gut

The gastrointestinal tract is organized along the anterior-posterior (A-P) axis from the esophagus to the anus, also referred to as the proximodistal axis. More specifically, the gut encompasses the small intestine at the anterior and the colon at the posterior end. Regionalization of the gut along the A-P axis is marked by differences in molecular, cellular, functional, and immune differences (Lickwar et al., 2017; Bowcutt et al., 2014; Suzuki, 2009; Cramer et al., 2015; Oehlers et al., 2011). In light of these distinctions, we first asked whether regional differences in the healthy adult gut along the A-P axis could be associated with apparent differences in the gut-residing macrophages. Using the regionalization schema that divides the length of the zebrafish gut into seven consecutive segments S1-S7 (Lickwar et al., 2017; Wang et al., 2010) comparable to other studies, we carefully examined the morphology and density of macrophages along the adult

zebrafish gut in these seven segments using high resolution *ex vivo* confocal imaging of dissected whole guts (Figure 1). We assessed the $m\phi$ -specific transgenic zebrafish line Tg(*mpeg1*:GFP) (Ellett et al., 2011) to visualize the macrophages (Figure 1). Interestingly, we found an increasing anterior-to-posterior gradient of macrophages in the adult gut starting from a relatively uniform density from S1-S4 to the highest density in the most posterior segment S7, which in zebrafish is homologous to the mammalian colon (Figure 1). We did not observe gross cell morphological differences along the segments, although the macrophages exhibited rather diverse morphologies in all gut regions. Similar to humans and rodents (Grainger et al., 2017), our analysis revealed that the colon-like region of the zebrafish gut contains the highest density of tissue-resident macrophages. These results implicate a possible conserved link between the high abundance of gut macrophages in the colon and the highest microbiota content (Dieterich et al., 2018).

Zebrafish harbor distinct mucosa- and muscularis-associated gut macrophages

While differences in gross cellular morphologies of gut macrophages were overall similar along the A-P axis, we next asked whether morphological differences could be observed between macrophages located in the different concentric layers of the gut starting from the center luminal side to the outer longitudinal muscle layer. Compared to their mammalian counterparts, zebrafish exhibit a somewhat simplified architectural organization. Rather than finger-like villi as in mammals, zebrafish have elongated and continuous ‘villar ridges’ that project into the luminal space and are lined with a single layer of intestinal epithelial cells mediating the environmental interface of the gut tube (Wallace et al., 2005). Zebrafish appear to lack a properly organized submucosal space (and associated submucosal neuronal networks), crypts, and have a relative reduction in the thickness and complexity of tissue compared to mammals. Similar to mammals, the gut wall contains two orthogonally positioned muscle layers (circular and longitudinal) which are found surrounding the myenteric plexus containing the intrinsic neurons of the enteric nervous system (ENS) and associated nerve tracts; rather than organized intestinal ganglia, neuronal bodies are found scattered as individuals or small groups (1-4 neurons) (Figure 2A). In order to determine whether zebrafish harbor a *bona fide* intestinal muscularis-associated $m\phi$ population, we developed a whole-mount high-resolution confocal imaging strategy aimed at interrogating these cells by focusing on the intestinal musculature of the *ex vivo* gut which was opened longitudinally and flattened and placed in the closest approximation to the microscope objective (Figure 2B). Imaging intestine derived from Tg(*mpeg1*:GFP) adults in this way, we observed distinct *mpeg1*⁺ cell populations in both the intestinal mucosa/lamina propria, as well as the muscularis (Figures 2C and 2D). Similar to mammalian counterparts, these muscularis-associated cells are morphologically distinct and arranged in a spatial pattern which appears to maximize neighbor-to-neighbor distance.

Using high resolution confocal imaging with Nyquist sampling, we further observed striking *mpeg1*^{GFP+} signal not only in the mucosal space but also in the circular muscle, myenteric plexus, and longitudinal muscle regions (Figure 2E). When cell processes were observed in the circular or longitudinal muscles, they were found to be extending in the same orientation as the muscle fibers (Figure 2E and data not shown).

Furthermore, our imaging analysis shows that the majority of mucosa-associated macrophages in the zebrafish gut are associated with the basolateral side of the intestinal epithelium within the lamina propria and in close proximity to neural projections within the intestinal ridges (Figures 2C, 2D, and S1). Studies detailing the neuroimmune interactions of mucosa-associated macrophages are largely lacking thus far, but zebrafish could serve as a powerful model for uncovering their functional roles.

Intestinal MM ϕ form an anatomically distinct population which span several layers, and are intimately associated with enteric neural processes

Expounding upon our observations of concentric layer characterization in Figure 2, we utilized depth-coded analysis of high-resolution confocal z stack micrographs of adult double Tg(*mpeg1*:GFP/*nbt*:dsRed) *ex vivo* intestine to visualize MM ϕ and to determine whether these *mpeg1*^{GFP+} cells comprised a *bona fide* spatially segregated and neuronally associated population within the muscularis. We confirmed this anatomically distinct regionalization (Figure 3A, top panel) and their proximity to enteric neural processes (Figure 3A, bottom panel). By sampling at a 0.5 μ m voxel depth, we were able to further clearly distinguish the striking spatial segregation of these two populations and also assess more completely the tissue residency pattern exhibited by the neural-process associated MM ϕ cells (Figure 3B).

Strikingly, we frequently observed *individual mpeg1*^{GFP+} MM ϕ associated with neural processes spanning the longitudinal muscle, the myenteric plexus, and the circular muscle and found that rather than inhabiting

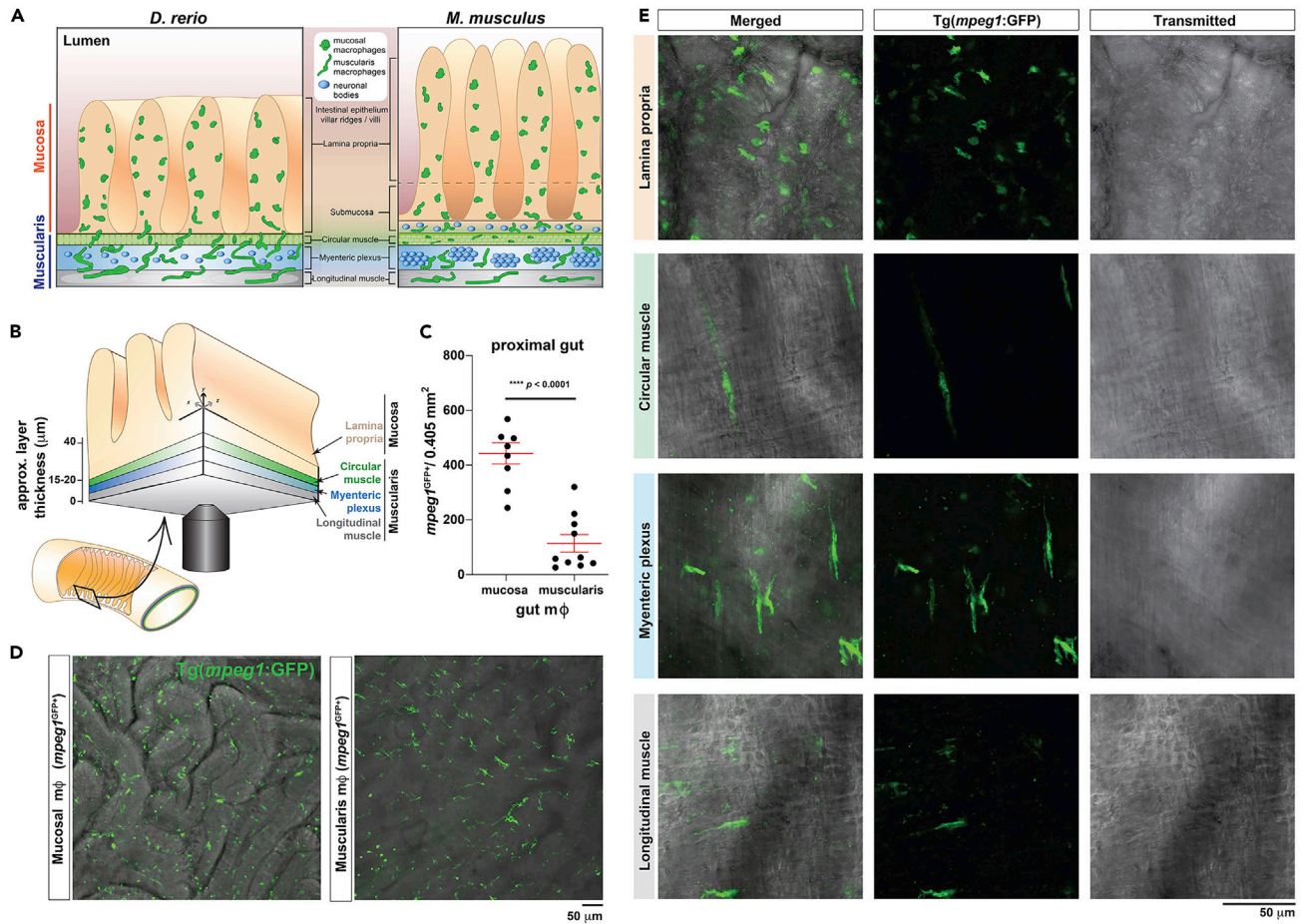


Figure 2. Zebrafish harbor distinct mucosa- and muscularis-associated intestinal macrophages

(A) Illustration depicts concentric anatomical layers of the proximal (small) intestine and associated macrophage populations in zebrafish (A, left) and mouse (A, right).

(B) Illustration depicts ex vivo imaging strategy with the muscularis positioned nearest the imaging objective.

(C and D) (C) Quantification of mucosa and muscularis-associated $mpeg1^{GFP+}$ macrophages in several fields of view per animal pooled from $n = 3$ Tg(*mpeg1*:GFP) adult ex vivo gut by region-specific z-projection as shown in (D) scale = 50 μm.

(E) Representative Nyquist-sampled confocal imaging micrographs (voxel depth 3 μm) highlighting regional diversity of mucosa- or muscularis-associated $mpeg1^{GFP+}$ fluorescence in the concentric layers of the gut: lamina propria, circular muscle, myenteric plexus, and longitudinal muscle. p value was determined by a two-tailed T test. Scale bars are shown as indicated.

See also Figure S1.

distinct anatomical niches within the muscularis (which is observed in mammals), MMφ frequently extend processes which span multiple layers of the gut wall (Figure 3C); six types of MMφ occupation were observed and type 2 being one of two most abundant categories representing MMφ that span across the entire muscularis (Figures 3C and S2). An individual MMφ can be observed to span the myenteric plexus and extend processes aligning with the longitudinal muscle and circular muscle layers on opposite sides of the cell body (Figures 3D, 3E, and S2). We confirmed the intimate macrophage interaction with neural processes found by *mpeg1*:GFP using an antibody-mediated approach with the pan-immune cell target L-plastin (Figure 3F). Similar to their mammalian counterparts, the gut muscularis of zebrafish appears to be immune-poor with the exception of *mpeg1*+ MMφ, whereas the mucosa exhibits a large density of L-plastin positive cells that are *mpeg1*- (data not shown).

In order to confirm the locational specificity of the MMφ within the muscularis and determine whether MMφ were intimately associated and extending processes along the densely packed smooth muscle, we used an antibody-retrieval mediated and secondary amplification approach using the Tg(*sm22*:GFP) (Seiler et al., 2010) reporter and primary antibodies raised against GFP and L-plastin. While we indeed observed

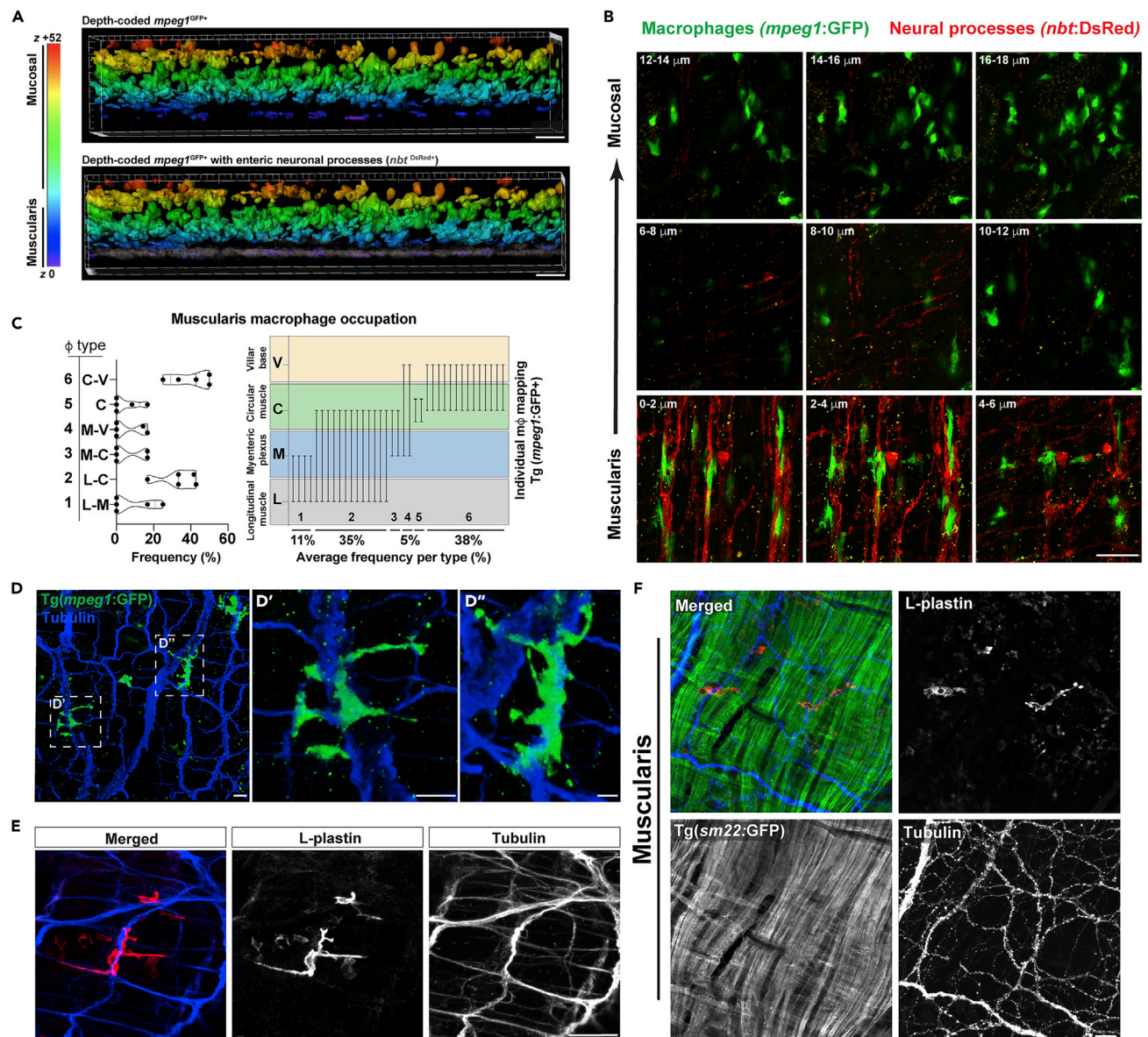


Figure 3. Zebrafish gut muscularis macrophages form an anatomically distinct population and intimately associate with neural processes

(A) Volumetric depth-coded analysis (Imaris) of 40 x confocal micrographs from $Tg(mpeg1:GFP;nbt:dsRed)$ *ex vivo* proximal adult gut highlighting a spatially distinct $mpeg1^{GFP+}$ MMφ population (purple, top panel) which co-segregate with dense nbt^{DsRed+} neural processes (gray, bottom panel). Data are representative of at least $n = 5$ animals.

(B) 2 μm confocal z series micrographs (0.5 μm voxel depth with Nyquist sampling) showing intimate $mpeg1^{GFP+}$ MMφ - nbt^{DsRed+} neural process associations.

(C–E) (C, left) Graphical representations of MMφ occupation frequencies spanning the longitudinal muscle – myenteric plexus (L–M), longitudinal muscle – circular muscle (L–C), myenteric plexus – circular muscle (M–C), myenteric plexus – villar ridge base (M–V), circular muscle (C), or circular muscle – villar ridge base (C–V) regions. (C, right) Graphical representations of end-to-end macrophage occupation across gut layers highlighting bridging MMφ phenotype. High-resolution confocal imaging with Nyquist sampling of *ex vivo* (D) $Tg(mpeg1:GFP)$ adult gut tissue (α -GFP, α -acetylated tubulin immunolabeled) highlight neural bridging of $mpeg1^{GFP+}$ MMφ processes and (E) wild-type adult gut tissue without Tg (α -L-plastin and α -acetylated tubulin immunolabeled) demonstrating Tg-independent visualization of MMφ-neural processes and interactions.

(F) *Ex vivo* $Tg(sm22:GFP)$ adult gut tissue was fixed and $sm22:GFP$, L-plastin, and acetylated tubulin were visualized by antibody-mediated immunolabeling to highlight specific MMφ associations with neural processes rather than smooth muscle fibers of the muscularis externa. Scale bars shown = 20 μm (A, F); 50 μm (B, E); 40 μm (D).

See also Figure S2.

MM ϕ presence between the smooth muscle layers, they did not morphologically mirror them or appear to be intimately in contact; conversely, MM ϕ appeared to extend cellular processes along intrinsic enteric neural tracts with which they specifically and intimately associate (Figures 3D and S2). These antibody-based antigen retrieval methods against GFP (to enhance signal quality and signal-to-noise ratio of the macrophage transgene) and acetylated tubulin coupled with our muscularis-focused high resolution confocal imaging strategy on fixed *ex vivo* gut tissue allowed us to observe the process extensions and intricate interactions of MM ϕ and intrinsic ENS neural tracts. We observed that *mpeg1*^{GFP+} MM ϕ frequently extend processes and can be observed bridging orthogonal neural processes located in oppositional circular and longitudinal muscularis layers (Figures 3E, 3F, and S2).

Combined *in vivo* and *ex vivo* imaging reveals emergence of abundant intestinal macrophages along the developing gut tube during the zebrafish larval period

To further examine macrophage association with the ENS, we next examined the developmental time course of the appearance of intestinal macrophages. We leveraged double transgenic zebrafish carrying both the macrophage and pan-neuronal transgenes (*mpeg1*:GFP and *nbt*:dsRed, respectively) to perform complementary *in vivo* whole mount and *ex vivo* whole gut imaging (Figure 4). These strategies led to consistent findings that provided a reliable understanding of the spatiotemporal appearance of gut-associated macrophages, as well as their close association with neuronal cells and processes in the developing gut tube from 3 dpf to 30 dpf (Figure 4).

During early larval development beginning at 3 days postfertilization (dpf, corresponding to ~3.5 mm standard length [SL]), around the time of hatching when the yolk has not fully resorbed, the nascent posterior intestinal tube becomes apparent (Figure 4A, dashed line). Even at this immature stage though rare in frequency, we observed gut-associated m ϕ (*mpeg1*:GFP) in intimate proximity to developing enteric neurons (*nbt*:dsRed) (Figure 4A, arrows). Outside the gut region, we observed striking m ϕ -neural tract interactions in the developing body (Figures 4B and 4B') that included intimate direct contact with the developing peripheral nervous system ganglia (Figure 4C).

By ~6 dpf the larval gut tube has organized, and the yolk has completely resorbed; these correlate with the onset of exogenous feeding, development of the swim bladder, and free swimming. The gut contains a robust neuronal population *nbt*-expressing enteric neurons and processes (Figure 4C). Extraintestinal m ϕ are found dispersed throughout the body, maintaining a striking association with the developing posterior lateral line, a mechanosensory organ critically important for detecting changes in water currents and environmentally informed movement (Figures 4C' and 4C''). Gut-associated macrophages increase in frequency and maintain intimate associations with the ENS (Figure 4C'''). At this stage of development, microsurgical procedures are feasible to obtain a full *ex vivo* intestinal preparation. This method allows for a close-up and definitive assessment of *bona fide* gut-residing m ϕ (Figure 4D) which rendered conventional *in vivo* whole-body imaging ambiguous due to the overlying skin-associated macrophages that can obstruct their distinction from the intestinal macrophages located superficially in the gut. Notably, these m ϕ exhibit fully mature and well-defined morphologies with highly branched often far-reaching processes, presumably enabling them to surveil a large tissue area (Figures 4E and 4E').

Around 9 dpf, the larvae undergo an intense period of growth and intestinal development. This is when a striking increase in colonization of macrophages in the gut alongside a larger network of neurons can be observed by *in vivo* and *ex vivo* imaging (Figures 4F–4H). This is also the time point at which the bright auto-fluorescence stemming from the S5 segment of the intestine (as depicted in Figure 1) becomes apparent (Figure 4G).

By 14 dpf, orthogonal views of *ex vivo* gut show a predominantly muscularis-associated population potentially capable of extending processes into the villar ridge space (Figure 4I) accompanied by a dramatic increase in the frequency of intestinal *mpeg1*^{GFP+} m ϕ as well as *nbt* + intestinal neurons (Figures 4J and 4K). During this time the emergence of macrophages that appear to associate with the intestinal mucosal space, including extending processes around and in between epithelial cells, also arise (Figure 4L, arrow).

Larval development is complete at the onset of the juvenile adult stage transition at ~30 dpf when the fish are typically ~1.0 cm SL. At this time point the zebrafish gut has adopted the stereotypical S-shape of the mature adult gut form with the two intestinal bends markedly apparent (Figure 4M),

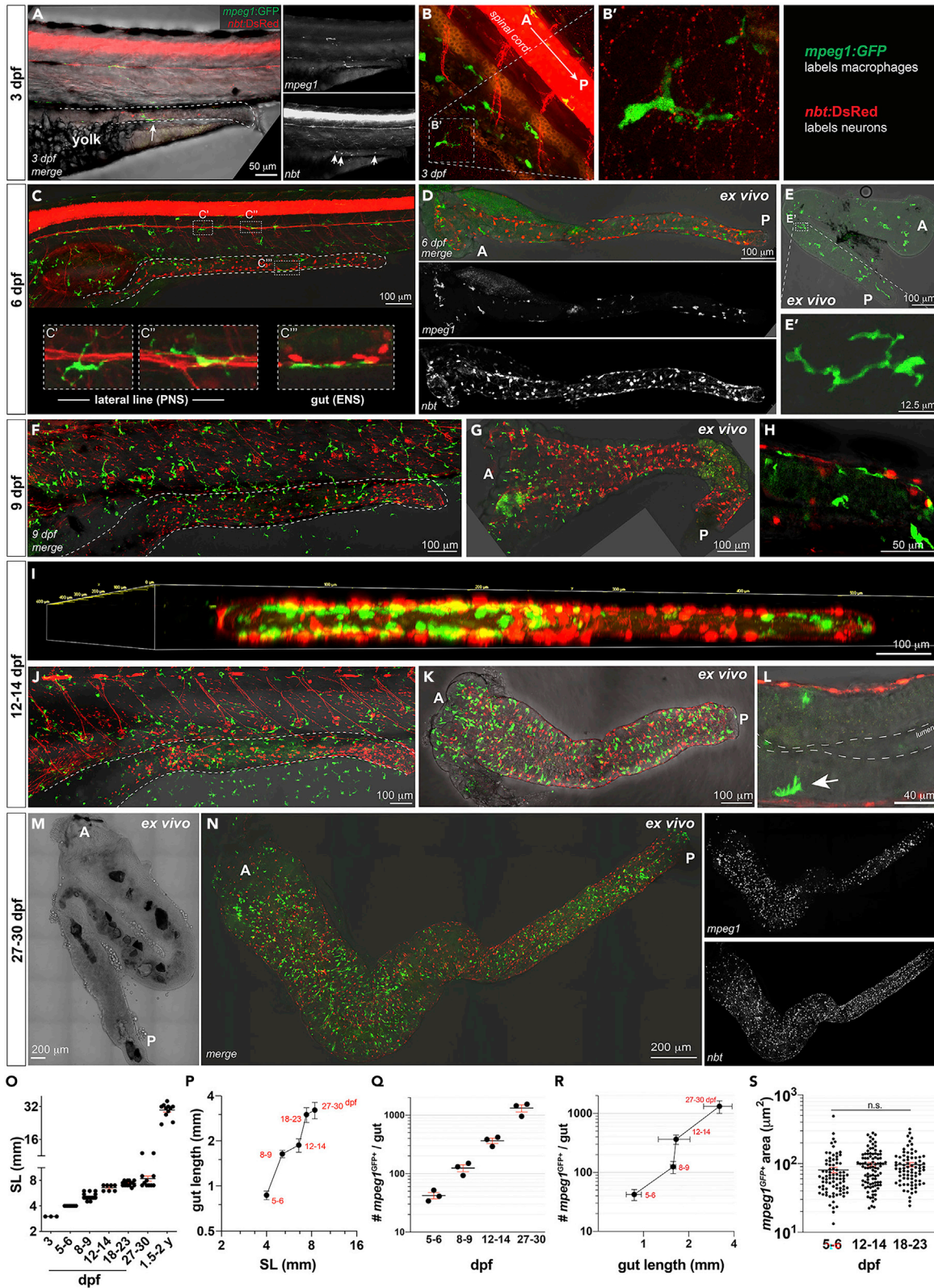


Figure 4. Spatiotemporal appearance and organization of gut macrophages from early larval to juvenile adult stages in zebrafish

- (A) Whole mount confocal (20X $z = 14$, 5 μm voxel depth) imaging of Tg(*mpeg1*:GFP; *nbt*:dsRed) at 3 dpf highlighting rare gut-associated *mpeg1*^{GFP+} m ϕ in proximity to maturing *nbt*^{DsRed+} gut neural tracts. Dashed line indicates margins of developing intestinal tube.
- (B) Outside of the gut, at 3 dpf m ϕ are often associated with neural processes of the peripheral nervous system (PNS) (20 X with Nyquist sampling $z = 25$, 2 μm voxel depth). (B') Inset shows m ϕ -neural process bridging (20 X with Nyquist sampling $z = 10$, 2 μm voxel depth).
- (C) Whole mount *in vivo* imaging of 5-6 dpf Tg(*mpeg1*:GFP;*nbt*:dsRed) fish reveals m ϕ are more frequently found throughout the body with increased gut-associated m ϕ frequency (20 X tiled image $z = 32$, 3 μm voxel depth). (C' and C'') M ϕ at this stage are well developed and often observed along the lateral line nerve where m ϕ bodies lie along the lateral line itself and m ϕ processes contact and bridge adjacent *nbt*^{DsRed+} neural processes. (C''') At 5-6 dpf gut *mpeg1*^{GFP+} m ϕ are *nbt*^{DsRed+}- associated in the enteric nervous system (ENS).
- (D–G) (D) *Ex vivo* intact whole gut explant confocal imaging (20 X tiled image, $z = 30$, 3 μm voxel depth) at 6 dpf showing distribution and location of macrophages (*mpeg1*^{GFP+}) and enteric neurons (*nbt*^{DsRed+}) along the intestine (A, anterior; and P, posterior), and (E) elaborately extended 'mature' and differentiated morphologies of gut-associated macrophages (20 X, $z = 8$, 3 μm voxel depth). Both *in vivo* whole mount imaging (20 X, $z = 18$, 5 μm voxel depth) (F) and *ex vivo* whole gut explant imaging (G) at 9 dpf shows increased density of gut macrophages relative to the distribution of neurons in the gut and along the body (20 X tiled image, $z = 20$, 5 μm voxel depth).
- (H) Higher magnification *in vivo* imaging shows contact between intestinal macrophages with enteric neuronal cell bodies and processes (20 X, $z = 16$, 5 μm voxel depth).
- (I) 3D volumetric rendering of 12-14 dpf *ex vivo* whole gut explant demonstrates increased density of *mpeg1*^{GFP+} m ϕ in the surrounding gut wall, suggesting a possible 'outside-in' development of gut macrophages (20 X, $z = 37$, 1 μm voxel depth).
- (J) Whole mount *in vivo* imaging of 12-14 dpf Tg(*mpeg1*:GFP;*nbt*:dsRed) fish shows increased density of whole-body and gut-associated *mpeg1*:GFP⁺ macrophages (20 X tiled image, $z = 50$, 5 μm voxel depth). Dotted lines demarcate the intestinal tube.
- (K) *Ex vivo* intact whole gut explant confocal imaging at 12-14 dpf shows gut-specific residency of dense *mpeg1*:GFP⁺ cells (20 X tiled image, $z = 16$, 5 μm voxel depth).
- (L) *mpeg1*^{GFP+} macrophages, arrow, can be seen abutting neuron-containing musculature and intercalating processes around intestinal epithelial cells (20 X with Nyquist sampling, $z = 15$, 1 μm voxel depth).
- (M) Transillumination imaging demonstrates stereotypical 'adult-like' S-shape of the gut becomes apparent around 30 dpf (20 X tiled image $z = 13$, 5 μm voxel depth).
- (N) The developed gut is densely innervated and populated with *mpeg1*^{GFP+} m ϕ and appears mature in phenotype (20 X tiled image $z = 17$, 5 μm voxel depth).
- (O) Standard length (mm) of zebrafish increases linearly across larval development. Pooled data are represented as average \pm S.E.M., $n = 3$ –20 per group.
- (P) Gut length increases as a function of development nonlinearly, with two 'spurts' of growth including between 6 and 9 days (just after complete yolk resorption and onset of exogenous feeding) and at the onset of the juvenile development stage (~3-4 weeks postfertilization).
- (Q) The number of total *mpeg1*^{GFP+} gut m ϕ at key stages of larval development increases exponentially as shown by a linear increase on a base ten logarithmic scale. Representative data ($n = 3$ /group) are shown as mean \pm S.E.M.; numbers show the average total macrophage number per gut.
- (R) Increase in total *mpeg1*^{GFP+} gut m ϕ as a function of gut length shows a similar developmental pattern as in (P) Representative data ($n = 3$ /group) are shown as mean \pm S.D.
- (S) Individual m ϕ area (μm^2) remains constant across larval development. Graph shows area calculations of $n = 20$ –40 individual macrophages pooled from $n = 3$ individuals at the indicated developmental checkpoints. Mean \pm S.E.M. is depicted, significance determined by one-way ANOVA. Q-S, log-linear plots shown on a base ten logarithmic scale on the y axis. A = anterior, P = posterior. Scale bars shown as indicated.
- See also [Figures S3](#) and [S4](#).

indicative of a major morphological event. Gut m ϕ populations begin to closely resemble that of adult fish ([Figure 4N](#)), with a distinct anatomical segregation and discernable morphological disparity between mucosa (villar ridge) associated- and muscularis-associated m ϕ ([Figure S3](#)). MM ϕ can be clearly observed between the smooth muscle layers and intimately associated with intrinsic enteric neural processes. They adopt elongated and often bridge-like morphologies, which are distinct from the mucosa-associated macrophages ([Figure S3](#)). Gut length increases non-linearly and mirrors the two major developmental post-embryonic periods, early larval (8-14 dpf) and late larval (18-30 dpf) stages ([Figure 4P](#)). Notably, gut m ϕ number increases exponentially during larval development as shown on a logarithmic scale ([Figure 4Q](#)), in parallel to the growth of gut length and body length (SL) ([Figure 4R](#)). We found that the average m ϕ cellular size across all stages of development assessed remained unchanged ([Figure 4S](#)), while the animal length, gut length, tissue thickness and complexity undergo substantial increases as the organism develops ([Figures 4O–4R](#)). This indicates that as the gut grows over time, there is an increase in either local proliferation or colonization of macrophages to account for the increase in macrophage density in the gut ([Figures 4](#) and [S4](#)). While intestinal macrophages appear more spread out across a larger gut length at early larval stages, they become more densely packed at later stages ([Figures 4](#) and [S4](#)). Since the intestinal macrophages do not significantly change in total cellular size over time ([Figure 4S](#)), the apparent wide span of early intestinal macrophages may reflect a possible larger relative gut length they patrol than compared with later stage intestinal macrophages. Together, these data demonstrate that intestinal macrophages are present in the larval zebrafish as early as 3 dpf, maintain intimate proximity to enteric neuronal cells and processes throughout development, and increase in density as the gut matures.

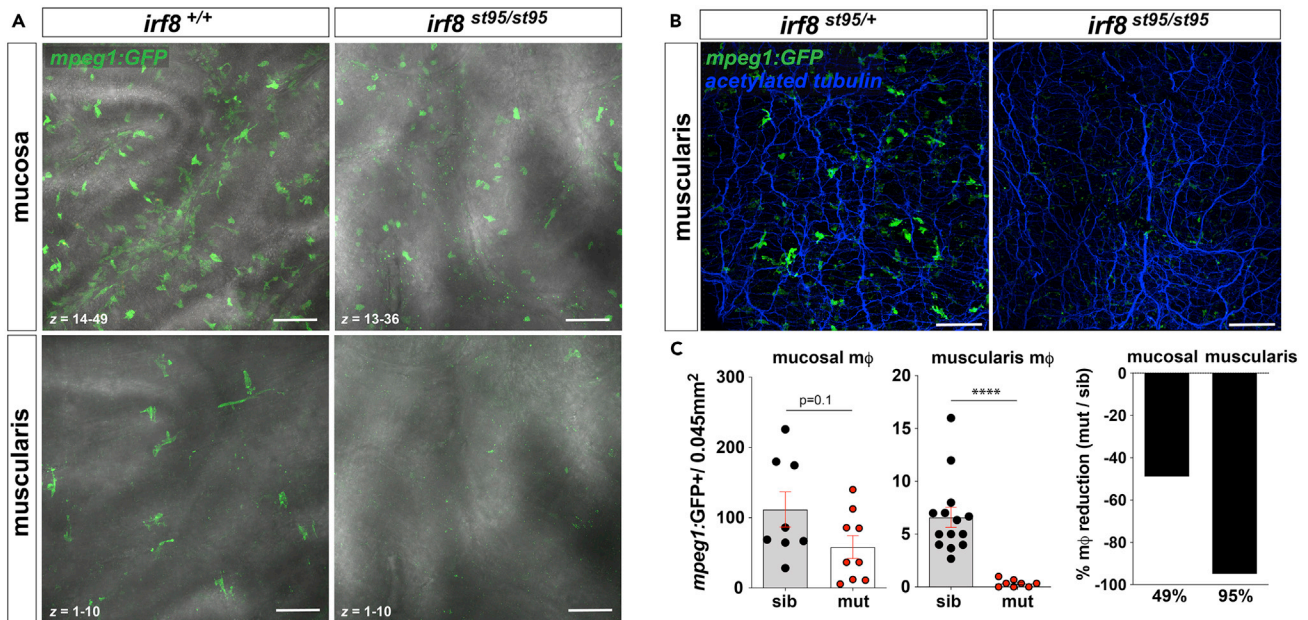


Figure 5. Genetic ablation of *irf8* causes a severe reduction in muscularis macrophages

(A) Representative confocal z stack micrographs of *ex vivo* *irf8*^{+/+} and *irf8*^{st95/st95} Tg(*mpeg1*:GFP) proximal gut tissue showing *irf8*-mediated mφ loss in both the mucosa (top) and muscularis (bottom) (40 X, 1 μm voxel depth).

(B) Representative confocal z stack micrographs of *ex vivo* *irf8*^{+/+} and *irf8*^{st95/st95} Tg(*mpeg1*:GFP) proximal gut-fixed tissue (anti-acetylated tubulin antibody retrieval) showing *irf8*-mediated neural process-associated MMφ loss in the muscularis (20 X, z = 16, 2 μm voxel depth).

(C) Quantification of *mpeg1*:GFP + cells in the mucosa (left) and muscularis (middle) of *irf8*^{st95/st95} mutants (mut) compared to wild-type or heterozygous siblings (sib) showing ~50% reduction in mucosal macrophages versus a 95% reduction of muscularis macrophages (right) from pooled non-overlapping confocal z stack micrographs (n = 3–4 individuals per group). More inter-individual variation was observed in frequency of mucosal macrophages which in part may be due to influence of the gut microbiota. Data shown are mean ± S.E.M. ****p < 0.0001 determined by nonparametric Mann-Whitney two-tailed T test. Data are representative of at least n = 3 adult individuals per group and at least 3 independent experiments. Scale bar = 100 μm.

See also [Figures S5](#) and [S6](#).

Genetic ablation of transcription factor *irf8* severely eliminates MMφ and affects intestinal transit during development

In light of the close association between intestinal macrophages with neural processes in the developing gut, we next determined whether perturbation of these macrophages would result in a gross intestinal functional defect. Since *irf8* deficiency in zebrafish has been shown to cause a drastic reduction in gut mφ without differentiating the gut macrophage subtypes ([Earley et al., 2018b](#)), we further characterized this loss in adult *irf8* mutants in more detail and indeed found a significant decrease in mucosa associated mφ (~50% reduction), and most dramatically in the muscularis subpopulation (95% reduction) ([Figure 5](#)). We further assessed this striking MMφ loss by employing a co-labeling strategy (L-plastin [red] and acetylated tubulin [blue]) and observed that the rare remaining MMφ in *irf8*^{st95/st95} mutants lack cell body extensions ([Figure S5](#)) and do not exhibit the typical wild type muscularis ‘bridging’ phenotype, where MMφ cellular processes span several gut layers ([Figure S2](#)). Though surviving mutant adults are phenotypically normal and do not appear to exhibit any overt developmental defects ([Figure S6A](#)) ([Earley et al., 2018b](#)), they consistently occur at a lower-than-Mendelian expected frequency in adult populations ([Figure S6B](#)). Since MMφ-enteric neuron crosstalk has been shown to regulate intestinal motility ([Muller et al., 2020](#)), we asked whether the MMφ loss seen in *irf8* mutants was correlated with changes in global intestinal transit but found that feeding capability and overall transit were unaffected in *irf8* mutant adults in the fasting or fed steady state condition ([Figure S6C](#)). By 48 hr after feeding, adult stage-matched fish of all genotypes were found to have excreted most ingested food; gut content level was not distinguishable between MMφ-depleted *irf8* mutants and their control heterozygous siblings which have wild-type MMφ at all timepoints (before feeding, during feeding, and 48 hr after feeding) ([Figure S6C](#)).

Since intestinal macrophages could differentially impact different stages of the gut, we further examined whether depletion of intestinal macrophages affected gut motility during development. We leveraged the

experimental strengths of the larval zebrafish at 10–11 dpf to conduct a longitudinal study of intestinal transit and gut motility following a number of individuals by *in vivo* imaging at a high tissue resolution (Figure 6). Surprisingly, in contrast to the results from the adult analysis, we found a significantly shorter intestinal transit time in the larval *irf8* mutant gut, but no significant difference in instantaneous gut motility as defined by peristaltic waves and rectal contractions (Kuil et al., 2020) captured in a 5-min high-speed time-lapse recording within 1 hr of feeding (Figure 6). These results along with the analysis conducted in adults indicate that intestinal macrophages (particularly MM ϕ) are not essential for routine intestinal muscle movements, but may importantly modulate the myenteric plexus and other components that control and coordinate the transit of food contents through the GI tract. Together, these results show that *irf8*-deficient mutants have a targeted severe loss of MM ϕ and significantly shorter gut transit time during development but no detectable change in adults.

DISCUSSION

Macrophage diversity in the zebrafish gut

Understanding the diversity of gut macrophages lays the critical foundation necessary for understanding gut m ϕ in maintenance of intestinal homeostasis and in disease processes. Whether zebrafish harbor a gut m ϕ diversity similar to that of mammals has remained unknown, and describing their heterogeneity remains a central key in understanding their use as a model organism for studies relevant to human health. This study provides anatomical evidence for morphological heterogeneity among zebrafish gut-associated m ϕ and characterizes a *bona fide* muscularis-associated MM ϕ population in the zebrafish gut. We also found these macrophages to be intimately associated with the gut tube neural tracts. Leveraging the m ϕ -specific Tg(*mpeg1*: GFP) zebrafish line and combining whole gut *ex vivo* tissue preparation with immunolabelling and high-resolution imaging techniques, we characterized the intestinal macrophages in detail along the anterior to posterior axis and the concentric layers of the adult zebrafish gut (Figures 1, 2, and 3), as well as their establishment across different developmental stages (Figure 4). We interrogated the appearance of neural- and gut-associated m ϕ at key stages of development and found that gut-associated m ϕ are present within the developing gut tube as early as 3 dpf, when neural differentiation of the ENS is in its nascency (Heanue et al., 2016). We also found morphologically distinct mucosal and MM ϕ at the larval to juvenile adult transition stage at around 27–30 dpf.

Bona fide MM ϕ bridge layers in the zebrafish gut wall

Using the macrophage- and pan-neuronal specific reporter lines and improved whole mount immuno-imaging techniques (Figure 2B), we demonstrated that, as in mammals, a subset of zebrafish m ϕ occupy the gut wall (within the intestinal muscularis) and are morphologically distinct and anatomically segregated from mucosal associated m ϕ (Figures 2C–2E). MM ϕ also exhibit stereotypical tissue-resident patterning (Figure 2D) and segregate with enteric neural processes (Figure 3A), suggesting possible functional interactions with the enteric neural network. In mice, MM ϕ appear to further segregate in each of the muscle layers (circular, longitudinal) and the myenteric plexus, where they adopt bipolar or stellate morphologies, respectively (Gabanyi et al., 2016). At first, these two distinct morphologies of MM ϕ (bipolar [circular or longitudinal muscle] and stellate [myenteric plexus]) appeared to be present in zebrafish (Figure 2E), however high-resolution imaging revealed that most MM ϕ exhibit a bridging phenotype where they traverse multiple orthogonal layers of the gut wall (Figures 3C–3F and S2). Notably, among MM ϕ , a majority of these cells resided in between the circular and longitudinal muscle, with cell body extensions in each layer and intimately wrapped around neural process extensions (Figures 3C–3F and S2) suggesting a role for MM ϕ in gut motility and coordinating smooth muscle contraction. The functional significance of the zebrafish MM ϕ bridging across the muscularis remains not known, but this may enable fewer MM ϕ to fulfill the essential macrophage functions in the gut, and that each macrophage cell may potentially be equipped to be more versatile and multi-functional than its mammalian counterpart. Alternatively, this bridging phenotype could simply reflect reduced cellular complexity of the gut wall tissue itself (Figure 2A). In mice, MM ϕ appear to congregate around enteric ganglia and neuronal bodies (Gabanyi et al., 2016) whereas this study provides evidence that MM ϕ of the zebrafish most frequently associate with neural projections and are rarely found associated with ENS neuronal cell bodies at steady state. This could be due to the fact that zebrafish lack organized ganglia in the myenteric plexus (Figure 2A) throughout life from development to adulthood (Flores et al., 2020; Kuil et al., 2020). Although the breadth of molecular and functional diversity remains to be fully characterized and the functional consequences of MM ϕ and neuronal interactions unclear, anatomical and morphological similarities suggest functional homology between zebrafish and mammalian MM ϕ likely exist.

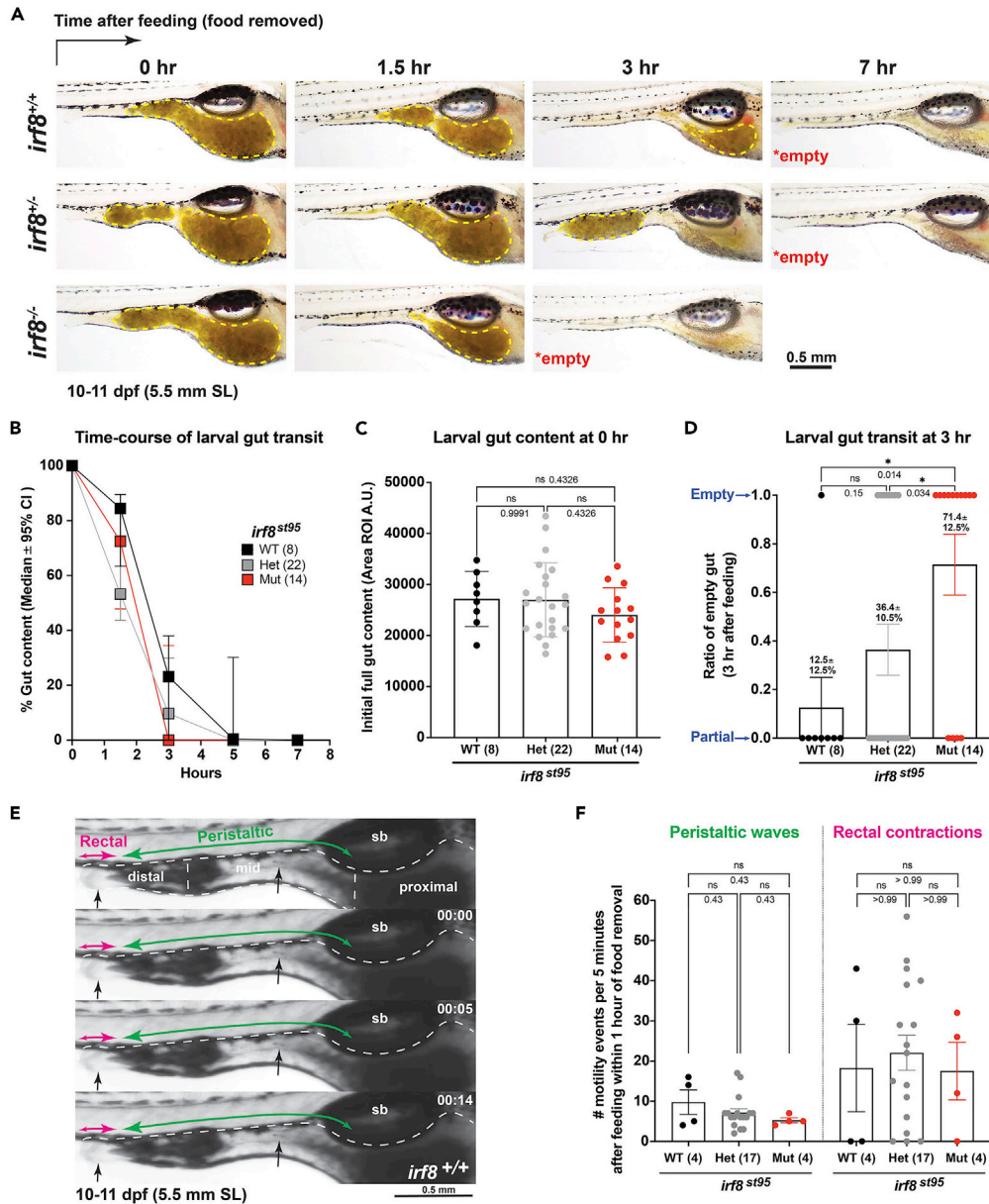


Figure 6. Severe depletion of intestinal macrophages in *irf8* mutants leads to faster intestinal transit during larval development

(A) Longitudinal analysis of intestinal transit in rotifer-fed larval zebrafish at 10-11 dpf (5.5 mm SL) indicates faster emptying of gut contents in *irf8* mutants, most by 3 hours (hr) after feeding and food withdrawal compared with 5-7 hr for control wild-type and heterozygous siblings. Color images of the gut, where food content is clearly visible (yellow dotted region), were taken at the specified time points for each individual tracked in real time. By 7 hr post feeding, all larvae were found to have empty guts.

(B) Time course plot showing median percentage of gut content and the 95% confidence interval (CI) for larval gut transit at 10-11 dpf. Most *irf8* mutants reach 0% gut content by 3 hr post feeding compared with siblings at 5-7 hr postfeeding. (C) Initial level of gut content indicates no significant difference in food intake in the different genotypes. Error bars show S.D.

(D) Analysis of the ratio or percentage of individual larvae with empty intestines at 3 hr postfeeding shows that *irf8* mutants have a significantly larger proportion at 71.4% compared with wild-type (12.5%) and heterozygous (36.4%) siblings. No significant difference was found between wild-type and heterozygotes. Error bars show S.E.M.

(E) Static monochromatic images extracted from a video recording of wild-type larval zebrafish gut motility. See also Videos S1, S2, and S3 for a representative recording of each genotype. Annotations show swim bladder (sb); three main

Figure 6. Continued

gut divisions (dotted regions): proximal for the intestinal bulb, midgut, and distal gut; and two major modes of motility (rectal contractions and peristaltic waves, both anterograde (mouth to anus) and retrograde (regurgitation) directions). Larger arrows indicate the predominant direction of the gut movement. Black arrows, sites of major gut movements. Timestamp in minutes: seconds. Scale bars shown as indicated.

(F) Scattered bar chart shows no significant difference in number of peristaltic waves and rectal contractions, although *irf8* mutants have a trend, although not significant, of reduced peristalsis. ns, not significant. Statistical significance was determined using one-way ANOVA test followed by multiple comparisons. Error bars show S.E.M. Each data point in plots C, D, and F represents an individual animal.

Mucosal macrophages appear as villar ridges develop and are associated with neural tracts in the mucosa

Our data also support the long-hypothesized and only recently evidenced association of mucosal $m\phi$ with villar neural projections (De Schepper et al., 2018) although our anatomical data suggests that many mucosal $m\phi$ may engage varicose villar neural projections rather than being a minority 'neuro-supportive' subset (Figure S1). We observed only rare *mpeg1*^{GFP} + cells that extend processes the full width of the epithelium, reminiscent of transepithelial dendrite extension into the lumen by dendritic cells (dendritic cells have not been described in zebrafish) (Chieppa et al., 2006; Rescigno et al., 2001). Moreover, we did not observe any *mpeg1*+ processes fully extending into the luminal space; our data support the notion that mucosal $m\phi$ at steady state may sample luminal contents indirectly, such as through endocytosis of budding epithelium rather than through direct means. Regardless of the specific mechanism, future investigations should explore the role that mucosal $m\phi$ play in luminal and tissue surveillance, and our data demonstrate that zebrafish could be a model for exploring these questions. Rather than finger-like villi, zebrafish harbors intestinal villar ridges similar to that of embryonic avian which develop in response to increasing metabolic demands of the growing animal (Burgess, 1975). Similar to our findings, the avian gut also exhibits two phases of growth (Burgess, 1975) suggesting that dedicated 'mucosal' macrophages may appear as a secondary feature of morphogenic invagination of the developing gut tissue.

This does not, however, fully explain the striking phenotypic change of the gut which appears to occur at the end of larval development beginning in the juvenile stage at ~27-30 dpf. More temporally fine resolution imaging coupled with transcriptional profiling of $m\phi$ across key stages of development would likely inform questions regarding the growth and age-related appearance of phenotypic muscularis and mucosal macrophages in the post-embryonic zebrafish. Additionally, direct comparisons of human, mouse, and zebrafish intestinal macrophages utilizing single-cell RNA-seq approaches may reveal understanding of important conserved molecular pathways governing individual macrophage cell identity and function in the gut. These types of studies promise to uncover transcriptionally based diversity of macrophages and point to anatomical niches that influence macrophage polarization, as has been recently described in humans (Bujko et al., 2018).

Interactions between microbiota, macrophages, and host gut tissue

The microbiota has been shown to regulate MM ϕ phenotypes (Muller et al., 2020). Conversely, we previously showed that zebrafish gut $m\phi$ can also regulate the composition of the intestinal microbiota (Earley et al., 2018b). Taken together, these data suggest a dynamic triologue among the gut microbiota, gut $m\phi$, and host gut tissue. The zebrafish model system could serve as an important tool in uncovering the nature of these interactions. Using a base ten semi-log plot, we found an exponential increase in the total number of intestinal $m\phi$ over developmental time that correlated with overall gut and animal size (Figure 4). It would therefore be interesting to further explore in zebrafish whether the gut $m\phi$ increase is a result of tissue development rather than the presumed microbial burden alone (Smith et al., 2011). Nonetheless, the differential frequency of $m\phi$ along the proximodistal axis found in the adult zebrafish gut (Figure 1) is consistent with the possibility of a conserved relationship between highest microbiota content with highest abundance of gut macrophages in the colon as that found in mammals (Dieterich et al., 2018).

MM ϕ appear dispensable for normal intestinal development and growth but affect developmental gastrointestinal transit

Studies have suggested that in adult animals, enteric neurons secrete survival factors necessary for MM ϕ maintenance (Muller et al., 2020); however, MM ϕ appear to colonize and pattern normally during development without neuronal dependency (Avetisyan et al., 2018). Conversely, depletion of long-lived tissue

resident m ϕ in mice has been recently shown to negatively impact enteric neuron survival and impair gut function and maintenance of homeostasis (De Schepper et al., 2018). It is unclear, however, whether the long-lived gut macrophages in mice pertains to only MM ϕ population. Our cursory observations from confocal imaging (Figure 5B) provide tentative data showing no gross abnormal enteric projections, but further detailed analyses are required to conclusively determine whether MM ϕ have a role in enteric neuronal maintenance, connections, or both in zebrafish. Furthermore, additional aspects such as the function or frequency of different intrinsic and extrinsic enteric neuronal subtypes that may be affected by MM ϕ are yet to be assessed (Kuil et al., 2020).

In humans, *IRF8* inactivating mutations cause immunodeficiency with a lack of circulating monocytes and dendritic cells (Hambleton, 2011), and the microglia of *Irf8*-deficient mice fail to initiate reactive (inflammatory) phenotypes in response to injury (Masuda et al., 2012). In zebrafish, *irf8* is differentially required for development of embryonic versus adult macrophages (Shiau et al., 2015). In this study, we further describe roles for *irf8* in the establishment, maintenance, and morphology of zebrafish gut m ϕ . We found that while *irf8* deficiency severely impacts gut macrophages (Figures 5 and S5), it preferentially depletes MM ϕ where we found that loss of *irf8* results in a near complete ablation of MM ϕ (95%) compared to just 50% of mucosal macrophages. However, this does not appear to impact the overall survivability of *irf8* mutants (Figure S6). Although there is an abundance of enteric neural-process associated MM ϕ in zebrafish, a severe depletion of these macrophages did not appear to impact instantaneous frequency of intestinal peristaltic waves and rectal contractions in the larval zebrafish (Figure 6), suggesting MM ϕ are not required for routine intestinal motility. However, total gut transit time was shorter in the MM ϕ -depleted *irf8* mutants during development with a possible trend of less peristalsis (although not significant) (Figure 6), implicating a modulating role for MM ϕ in the neural control of intestinal motility. Many parameters, such as directionality, strength, duration, speed, and coordination of the intestinal muscle movements that in part are controlled by the ENS, collectively determine how quickly digested food is pushed through the digestive tract. The process of gut transit is therefore an integrative outcome of multiple highly complex inputs. Future analysis of these different inputs that govern intestinal movements will better define the mechanisms by which MM ϕ affect developmental gut transit.

Although no significant change in gut transit was found in *irf8* mutants at the adult stage, small differences may not be detectable by the gross and cross-sectional analysis we conducted on different individuals at each time point, which is currently the most feasible approach in the adult zebrafish. Alternatively, MM ϕ may differentially impact gut motility in development and adulthood. Previous studies in mice implicated a role for MM ϕ in regulating gut motility based on effects of MM ϕ deficiency on total transit time; however the data yielded mixed results (De Schepper et al., 2018; Muller et al., 2020). Using diphtheria toxin-based depletion of *Cx3cr1*⁺ of intestinal M ϕ , prolonged gut transit time with no effect on stomach emptying was found (De Schepper et al., 2018), while no significant effect on total gut transit time but with accelerated stomach emptying and increased colonic transit time were observed in a selective depletion of at least 80% of MM ϕ using blocking anti-CSF1R antibody without affecting mucosal M ϕ (Muller et al., 2020). Since zebrafish lack a stomach (Lopez Nadal et al., 2020) and have a simpler gastrointestinal tract structure, the total transit time may more closely reflect overall gut motility, or the process of stomach emptying. Our study indicates a significant effect in total gut transit time in the developing zebrafish but not in adult zebrafish due to MM ϕ depletion, suggesting a possible impact of MM ϕ on the ENS-controlled coordination of gut motility during development. However, we cannot eliminate the possibility that MM ϕ may regulate gut motor functions in adult zebrafish at a more detailed level, including peristaltic contractions and patterns of gut movements. Furthermore, the influence of MM ϕ not only on fine muscle coordination in the normal adult gut, but also on gut motility in the diseased or otherwise stressed gut is yet unknown.

Developmental origin of zebrafish mucosal and MM ϕ remains an open question

Importantly, our study has not addressed the origin of the mucosal or MM ϕ we have described herein. As discussed earlier, tissue macrophages, including those of the gut, were thought to be derived entirely from circulating monocytes (Cohn, 1968). Recent fate-mapping studies (Cohn, 1968) have demonstrated that in mice a long-lived pool of macrophages does indeed exist, but the respective contributions of circulating monocytes vs. embryonically seeded long-lived tissue resident macrophages to the mucosal and muscularis populations are yet unknown. Macrophage cell lineage tracing strategies will be needed to address the developmental origin of mucosal and MM ϕ , and whether *irf8* dependency is associated with a distinct origin (primitive versus definitive) as previously implicated in zebrafish (Shiau et al., 2015).

CONCLUSIONS

In summary, we report critical advances in understanding the organization, distribution, and diversity of the zebrafish gut macrophages during development and in adults. Our study shows that zebrafish can be powerfully leveraged for direct interrogation of macrophage-centric neuroimmune interactions in the whole gut. In line with this, studies supporting their utility in understanding pathophysiology and cellular mechanisms related to gastrointestinal biology, mucosal immunology, and neuroimmunology have been recently increasing (Kuil et al., 2020; Flores et al., 2020; Earley et al., 2018b; Wang et al., 2010; Lickwar et al., 2017; Yang et al., 2020). Owing to the accessibility of the whole gut for high resolution given the thin nature of the gut tissue, we can acquire detailed imaging of the different cells along all dimensions of the gut which would be more difficult to achieve in other vertebrate models. The imaging analysis from this work establishes the presence of diverse intestinal macrophage subsets, namely muscularis and mucosal macrophages, in zebrafish similar to their mammalian counterparts, as well as reveals the nature of MM ϕ that span multiple gut layers and intimately make contacts with enteric neural processes. While the functional significance of individual MM ϕ bridging multiple layers of the gut wall remains unknown, their residency implicates their potential to exert broad effects that may be more versatile than their mammalian counterparts which are typically restricted to a single layer. These results motivate further work in examining the functional diversity and significance of intestinal macrophages and their interaction with the ENS which remain incompletely understood.

STAR★METHODS

Detailed methods are provided in the online version of this paper and include the following:

- KEY RESOURCES TABLE
- RESOURCE AVAILABILITY
 - Lead contact
 - Materials availability
 - Data and code availability
- EXPERIMENTAL MODEL AND SUBJECT DETAILS
 - Zebrafish husbandry and lines
- METHOD DETAILS
 - Tissue preparation and immunostaining
 - Quantification of gut macrophages and measurements of body/gut lengths
 - Classification of the MM ϕ occupation
 - Larval intestinal transit and motility assessments
 - Adult gut transit assessment
 - Vibratome sectioning
 - Imaging and Image Analysis
- QUANTIFICATION AND STATISTICAL ANALYSIS
- ADDITIONAL RESOURCES

SUPPLEMENTAL INFORMATION

Supplemental information can be found online at <https://doi.org/10.1016/j.isci.2021.102496>.

ACKNOWLEDGMENTS

The authors would like to thank members of the Shiao lab for fruitful discussions, and Michelle Altemara and all staff at the UNC Zebrafish Aquaculture Core Facility for fish care. The authors are grateful to Michael Pack for sharing transgenic fish, and Hiroyuki Kato for generous use of vibratome. C.L.G. was funded by the NIH T32 Training Grant 5T32AI007273 and received helpful feedback from T32 committee members Roland Tish and Scott Magness. This work was supported by NIH NIGMS grant R35GM124719 to C.E.S.

AUTHOR CONTRIBUTIONS

C.L.G. and C.E.S. conceived the study and designed experiments. C.L.G., V.K., and A.C. performed experiments and analyzed data. C.L.G. prepared figures, illustrations and wrote the manuscript. V.K. conducted larval gut motility and transit experiments, data analysis, and prepared Videos and figures. A.C. helped prepare figures, illustrations, and writing the manuscript. C.E.S. prepared figures, edited and wrote the manuscript, analyzed data, secured funding, and supervised this study. All authors reviewed and edited the manuscript.

DECLARATION OF INTERESTS

The authors declare no competing interests.

Received: November 20, 2020

Revised: March 17, 2021

Accepted: April 28, 2021

Published: June 25, 2021

REFERENCES

- Avetisyan, M., Rood, J.E., Huerta Lopez, S., Sengupta, R., Wright-Jin, E., Dougherty, J.D., Behrens, E.M., and Heuckeroth, R.O. (2018). Muscularis macrophage development in the absence of an enteric nervous system. *Proc. Natl. Acad. Sci. U S A* 115, 4696–4701. <https://doi.org/10.1073/pnas.1802490115>.
- Bilzer, M., Roggel, F., and Gerbes, A.L. (2006). Role of Kupffer cells in host defense and liver disease. *Liver Int.* 26, 1175–1186. <https://doi.org/10.1111/j.1478-3231.2006.01342.x>.
- Bowcutt, R., Forman, R., Glymenaki, M., Carding, S.R., Else, K.J., and Cruickshank, S.M. (2014). Heterogeneity across the murine small and large intestine. *World J. Gastroenterol.* 20, 15216–15232. <https://doi.org/10.3748/wjg.v20.i41.15216>.
- Brugman, S. (2016). The zebrafish as a model to study intestinal inflammation. *Dev. Comp. Immunol.* 64, 82–92. <https://doi.org/10.1016/j.dci.2016.02.020>.
- Bujko, A., Atlasy, N., Landsverk, O.J.B., Richter, L., Yaqub, S., Horneland, R., Oyen, O., Aandahl, E.M., Aabakken, L., Stunnenberg, H.G., et al. (2018). Transcriptional and functional profiling defines human small intestinal macrophage subsets. *J. Exp. Med.* 215, 441–458. <https://doi.org/10.1084/jem.20170057>.
- Burgess, D.R. (1975). Morphogenesis of intestinal villi. II. Mechanism of formation of previllous ridges. *J. Embryol. Exp. Morphol.* 34, 723–740.
- Chieppa, M., Rescigno, M., Huang, A.Y., and Germain, R.N. (2006). Dynamic imaging of dendritic cell extension into the small bowel lumen in response to epithelial cell TLR engagement. *J. Exp. Med.* 203, 2841–2852. <https://doi.org/10.1084/jem.20061884>.
- Choi, K.M., Kashyap, P.C., Dutta, N., Stoltz, G.J., Ordog, T., Shea Donohue, T., Bauer, A.J., Linden, D.R., Szszewski, J.H., Gibbons, S.J., et al. (2010). CD206-positive M2 macrophages that express heme oxygenase-1 protect against diabetic gastroparesis in mice. *Gastroenterology* 138, 2399–2409. <https://doi.org/10.1053/j.gastro.2010.02.014>.
- Cohn, Z.A. (1968). The structure and function of monocytes and macrophages. *Adv. Immunol.* 9, 163–214. [https://doi.org/10.1016/s0065-2776\(08\)60443-5](https://doi.org/10.1016/s0065-2776(08)60443-5).
- Cramer, J.M., Thompson, T., Geskin, A., Laframboise, W., and Lagasse, E. (2015). Distinct human stem cell populations in small and large intestine. *PLoS One* 10, e0118792. <https://doi.org/10.1371/journal.pone.0118792>.
- Darrow, K.O., and Harris, W.A. (2004). Characterization and development of courtship in zebrafish, *Danio rerio*. *Zebrafish* 1, 40–45. <https://doi.org/10.1089/154585404774101662>.
- Davies, L.C., Jenkins, S.J., Allen, J.E., and Taylor, P.R. (2013). Tissue-resident macrophages. *Nat. Immunol.* 14, 986–995. <https://doi.org/10.1038/ni.2705>.
- De Schepper, S., Verheijden, S., Aguilera-Lizarraga, J., Viola, M.F., Boesmans, W., Stakenborg, N., Voytyuk, I., Schmidt, I., Boeckx, B., Dierckx De Casterle, I., et al. (2018). Self-maintaining gut macrophages are essential for intestinal homeostasis. *Cell* 175, 400–415 e13. <https://doi.org/10.1016/j.cell.2018.07.048>.
- Dieterich, W., Schink, M., and Zopf, Y. (2018). Microbiota in the gastrointestinal tract. *Med. Sci. (Basel)* 6, 116. <https://doi.org/10.3390/medsci6040116>.
- Dixon, L.J., Barnes, M., Tang, H., Pritchard, M.T., and Nagy, L.E. (2013). Kupffer cells in the liver. *Compr. Physiol.* 3, 785–797. <https://doi.org/10.1002/cphy.c120026>.
- Doebel, T., Voisin, B., and Nagao, K. (2017). Langerhans cells - the macrophage in dendritic cell clothing. *Trends Immunol.* 38, 817–828. <https://doi.org/10.1016/j.it.2017.06.008>.
- Earley, A.M., Dixon, C.T., and Shiao, C.E. (2018a). Genetic analysis of zebrafish homologs of human FOXQ1, foxq1a and foxq1b, in innate immune cell development and bacterial host response. *PLoS One* 13, e0194207. <https://doi.org/10.1371/journal.pone.0194207>.
- Earley, A.M., Graves, C.L., and Shiao, C.E. (2018b). Critical role for a subset of intestinal macrophages in shaping gut microbiota in adult zebrafish. *Cell Rep.* 25, 424–436. <https://doi.org/10.1016/j.celrep.2018.09.025>.
- Elhelu, M.A. (1983). The role of macrophages in immunology. *J. Natl. Med. Assoc.* 75, 314–317.
- Ellett, F., Pase, L., Hayman, J.W., Andrianopoulos, A., and Lieschke, G.J. (2011). mpeg1 promoter transgenes direct macrophage-lineage expression in zebrafish. *Blood* 117, 49–56. <https://doi.org/10.1182/blood-2010-10-314120>.
- Epelman, S., Lavine, K.J., and Randolph, G.J. (2014). Origin and functions of tissue macrophages. *Immunity* 41, 21–35. <https://doi.org/10.1016/j.immuni.2014.06.013>.
- Flores, E.M., Nguyen, A.T., Odem, M.A., Eisenhoffer, G.T., and Krachler, A.M. (2020). The zebrafish as a model for gastrointestinal tract-microbe interactions. *Cell Microbiol.* 22, e13152. <https://doi.org/10.1111/cmi.13152>.
- Gabanyi, I., Muller, P.A., Feighery, L., Oliveira, T.Y., Costa-Pinto, F.A., and Mucida, D. (2016). Neuro-immune interactions drive tissue programming in intestinal macrophages. *Cell* 164, 378–391. <https://doi.org/10.1016/j.cell.2015.12.023>.
- Ginhoux, F., and Guillemins, M. (2016). Tissue-resident macrophage ontogeny and homeostasis. *Immunity* 44, 439–449. <https://doi.org/10.1016/j.immuni.2016.02.024>.
- Goldsmith, J.R., and Jobin, C. (2012). Think small: zebrafish as a model system of human pathology. *J. Biomed. Biotechnol.* 2012, 817341. <https://doi.org/10.1155/2012/817341>.
- Gomez Perdiguero, E., Klapproth, K., Schulz, C., Busch, K., Azzoni, E., Crozet, L., Garner, H., Trouillet, C., De Bruijn, M.F., Geissmann, F., et al. (2015). Tissue-resident macrophages originate from yolk-sac-derived erythro-myeloid progenitors. *Nature* 518, 547–551. <https://doi.org/10.1038/nature13989>.
- Grainger, J.R., Konkel, J.E., Zangerle-Murray, T., and Shaw, T.N. (2017). Macrophages in gastrointestinal homeostasis and inflammation. *Pflugers Arch.* 469, 527–539. <https://doi.org/10.1007/s00424-017-1958-2>.
- Hambleton, Sophie, et al. (2011). *IRF8* Mutations and Human Dendritic-Cell Immunodeficiency. *N Engl J Med.* 365, 127–138.
- Harry, G.J. (2013). Microglia during development and aging. *Pharmacol. Ther.* 139, 313–326. <https://doi.org/10.1016/j.pharmthera.2013.04.013>.
- Heanue, T.A., Shepherd, I.T., and Burns, A.J. (2016). Enteric nervous system development in avian and zebrafish models. *Dev. Biol.* 417, 129–138. <https://doi.org/10.1016/j.ydbio.2016.05.017>.
- Jutila, M.A., and Banks, K.L. (1986). Locally dividing macrophages in normal and inflamed mammary glands. *Clin. Exp. Immunol.* 66, 615–624.
- Krenkel, O., and Tacke, F. (2017). Liver macrophages in tissue homeostasis and disease. *Nat. Rev. Immunol.* 17, 306–321. <https://doi.org/10.1038/nri.2017.11>.
- Kuil, L.E., Chauhan, R.K., Cheng, W.W., Hofstra, R.M.W., and Alves, M.M. (2020). Zebrafish: a model organism for studying enteric nervous system development and disease. *Front. Cell Dev. Biol.* 8, 629073. <https://doi.org/10.3389/fcell.2020.629073>.
- Lavin, Y., and Merad, M. (2013). Macrophages: gatekeepers of tissue integrity. *Cancer Immunol.*

- Res. 1, 201–209. <https://doi.org/10.1158/2326-6066.CIR-13-0117>.
- Lavin, Y., Mortha, A., Rahman, A., and Merad, M. (2015). Regulation of macrophage development and function in peripheral tissues. *Nat. Rev. Immunol.* 15, 731–744. <https://doi.org/10.1038/nri3920>.
- Lickwar, C.R., Camp, J.G., Weiser, M., Cocchiari, J.L., Kingsley, D.M., Furey, T.S., Sheikh, S.Z., and Rawls, J.F. (2017). Genomic dissection of conserved transcriptional regulation in intestinal epithelial cells. *PLoS Biol.* 15, e2002054. <https://doi.org/10.1371/journal.pbio.2002054>.
- Lopez Nadal, A., Ikeda-Ohtsubo, W., Sipkema, D., Peggs, D., Mcgurk, C., Forlenza, M., Wiegertjes, G.F., and Brugman, S. (2020). Feed, microbiota, and gut immunity: using the zebrafish model to understand fish health. *Front. Immunol.* 11, 114. <https://doi.org/10.3389/fimmu.2020.00114>.
- Lu, J.W., Ho, Y.J., Ciou, S.C., and Gong, Z. (2017). Innovative disease model: zebrafish as an in vivo platform for intestinal disorder and tumors. *Biomedicine* 5, 58. <https://doi.org/10.3390/biomedicine5040058>.
- Masuda, T., Tsuda, M., Yoshinaga, R., Tozaki-Saitoh, H., Ozato, K., Tamura, T., and Inoue, K. (2012). IRF8 is a critical transcription factor for transforming microglia into a reactive phenotype. *Cell Rep.* 1, 334–340. <https://doi.org/10.1016/j.celrep.2012.02.014>.
- Matheis, F., Muller, P.A., Graves, C.L., Gabanyi, I., Kerner, Z.J., Costa-Borges, D., Ahrends, T., Rosenstiel, P., and Mucida, D. (2020). Adrenergic signaling in muscularis macrophages limits infection-induced neuronal loss. *Cell* 180, 64–78 e16. <https://doi.org/10.1016/j.cell.2019.12.002>.
- Mcdole, J.R., Wheeler, L.W., Mcdonald, K.G., Wang, B., Konjufca, V., Knoop, K.A., Newberry, R.D., and Miller, M.J. (2012). Goblet cells deliver luminal antigen to CD103+ dendritic cells in the small intestine. *Nature* 483, 345–349. <https://doi.org/10.1038/nature10863>.
- Mikkelsen, H.B. (1995). Macrophages in the external muscle layers of mammalian intestines. *Histol. Histopathol.* 10, 719–736.
- Mikkelsen, H.B. (2010). Interstitial cells of Cajal, macrophages and mast cells in the gut musculature: morphology, distribution, spatial and possible functional interactions. *J. Cell. Mol. Med.* 14, 818–832. <https://doi.org/10.1111/j.1582-4934.2010.01025.x>.
- Morales, R.A., and Allende, M.L. (2019). Peripheral macrophages promote tissue regeneration in zebrafish by fine-tuning the inflammatory response. *Front. Immunol.* 10, 253. <https://doi.org/10.3389/fimmu.2019.00253>.
- Muller, P.A., Matheis, F., and Mucida, D. (2020). Gut macrophages: key players in intestinal immunity and tissue physiology. *Curr. Opin. Immunol.* 62, 54–61. <https://doi.org/10.1016/j.coi.2019.11.011>.
- Oehlers, S.H., Flores, M.V., Chen, T., Hall, C.J., Crosier, K.E., and Crosier, P.S. (2011). Topographical distribution of antimicrobial genes in the zebrafish intestine. *Dev. Comp. Immunol.* 35, 385–391. <https://doi.org/10.1016/j.dci.2010.11.008>.
- Okabe, Y., and Medzhitov, R. (2016). Tissue biology perspective on macrophages. *Nat. Immunol.* 17, 9–17. <https://doi.org/10.1038/ni.3320>.
- Paolicelli, R.C., Bolasco, G., Pagani, F., Maggi, L., Scianni, M., Panzanelli, P., Giustetto, M., Ferreira, T.A., Guiducci, E., Dumas, L., et al. (2011). Synaptic pruning by microglia is necessary for normal brain development. *Science* 333, 1456–1458. <https://doi.org/10.1126/science.1202529>.
- Renshaw, S.A., and Trede, N.S. (2012). A model 450 million years in the making: zebrafish and vertebrate immunity. *Dis. Model. Mech.* 5, 38–47. <https://doi.org/10.1242/dmm.007138>.
- Rescigno, M., Urbano, M., Valzania, B., Francolini, M., Rotta, G., Bonasio, R., Granucci, F., Kraehenbuhl, J.P., and Ricciardi-Castagnoli, P. (2001). Dendritic cells express tight junction proteins and penetrate gut epithelial monolayers to sample bacteria. *Nat. Immunol.* 2, 361–367. <https://doi.org/10.1038/86373>.
- Rubino, S.J., Mayo, L., Wimmer, I., Siedler, V., Brunner, F., Hametner, S., Madi, A., Lanser, A., Moreira, T., Donnelly, D., et al. (2018). Acute microglia ablation induces neurodegeneration in the somatosensory system. *Nat. Commun.* 9, 4578. <https://doi.org/10.1038/s41467-018-05929-4>.
- Sawada, M. (1999). Brain cytokine network and novel characteristics of microglia. *Nihon Shinkai Seishin Yakurigaku Zasshi* 19, 151–154.
- Schenk, M., and Mueller, C. (2007). Adaptations of intestinal macrophages to an antigen-rich environment. *Semin. Immunol.* 19, 84–93. <https://doi.org/10.1016/j.smim.2006.09.002>.
- Seiler, C., Abrams, J., and Pack, M. (2010). Characterization of zebrafish intestinal smooth muscle development using a novel sm22alpha-b promoter. *Dev. Dyn.* 239, 2806–2812. <https://doi.org/10.1002/dvdy.22420>.
- Shaw, T.N., Houston, S.A., Wemyss, K., Bridgeman, H.M., Barbera, T.A., Zangerle-Murray, T., Strangward, P., Ridley, A.J.L., Wang, P., Tamoutounour, S., et al. (2018). Tissue-resident macrophages in the intestine are long lived and defined by Tim-4 and CD4 expression. *J. Exp. Med.* 215, 1507–1518. <https://doi.org/10.1084/jem.20180019>.
- Shiau, C.E., Kaufman, Z., Meireles, A.M., and Talbot, W.S. (2015). Differential requirement for irf8 in formation of embryonic and adult macrophages in zebrafish. *PLoS One* 10, e0117513. <https://doi.org/10.1371/journal.pone.0117513>.
- Shiau, C.E., Monk, K.R., Joo, W., and Talbot, W.S. (2013). An anti-inflammatory NOD-like receptor is required for microglia development. *Cell Rep.* 5, 1342–1352. <https://doi.org/10.1016/j.celrep.2013.11.004>.
- Smith, P.D., Smythies, L.E., Shen, R., Greenwell-Wild, T., Gliozzi, M., and Wahl, S.M. (2011). Intestinal macrophages and response to microbial encroachment. *Mucosal Immunol.* 4, 31–42. <https://doi.org/10.1038/mi.2010.66>.
- Suzuki, H. (2009). Differences in intraepithelial lymphocytes in the proximal, middle, distal parts of small intestine, cecum, and colon of mice. *Immunol. Invest.* 38, 780–796. <https://doi.org/10.3109/08820130903258800>.
- Wallace, K.N., Akhter, S., Smith, E.M., Lorent, K., and Pack, M. (2005). Intestinal growth and differentiation in zebrafish. *Mech. Dev.* 122, 157–173. <https://doi.org/10.1016/j.mod.2004.10.009>.
- Wang, Z., Du, J., Lam, S.H., Mathavan, S., Matsudaira, P., and Gong, Z. (2010). Morphological and molecular evidence for functional organization along the rostrocaudal axis of the adult zebrafish intestine. *BMC Genomics* 11, 392. <https://doi.org/10.1186/1471-2164-11-392>.
- Wehner, S., Behrendt, F.F., Lyutenski, B.N., Lysson, M., Bauer, A.J., Hirner, A., and Kalff, J.C. (2007). Inhibition of macrophage function prevents intestinal inflammation and postoperative ileus in rodents. *Gut* 56, 176–185. <https://doi.org/10.1136/gut.2005.089615>.
- Yang, L., Jimenez, J.A., Earley, A.M., Hamlin, V., Kwon, V., Dixon, C.T., and Shiau, C.E. (2020). Drainage of inflammatory macromolecules from the brain to periphery targets the liver for macrophage infiltration. *Elife* 9, e58191. <https://doi.org/10.7554/eLife.58191>.
- Zhao, X., and Pack, M. (2017). Modeling intestinal disorders using zebrafish. *Methods Cell Biol.* 138, 241–270. <https://doi.org/10.1016/bs.mcb.2016.11.006>.

STAR★METHODS

KEY RESOURCES TABLE

REAGENT or RESOURCE	SOURCE	IDENTIFIER
Antibodies		
Chicken α -GFP pAb	Abcam	Ab13970 (1:500)
AlexaFluor 488 goat anti-chicken IgY (H+L)	Abcam	Ab150169 (1:500)
Rabbit α -L-plastin		Reference: Redd et al. 2006 ⁶⁵
AlexaFluor 594 goat anti-rabbit IgG (H+L)	ThermoFisher	A11012 (1:500)
Mouse α -acetylated tubulin	Sigma Aldrich	clone 6-11B-1 (T7451) 1:500
AlexaFluor 350 goat anti-mouse IgG (H+L)	ThermoFisher	A11045 (1:500)
Mouse α -HuC/HuD neuronal protein (clone 16A11)	ThermoFisher	A21271 (1:250)
AlexaFluor 647 goat anti-mouse IgG (H+L)	ThermoFisher	A28181 (1:500)
Chemicals, peptides, and recombinant proteins		
Tricaine (Ethyl-3-aminobenzoate methanesulfonate)	Sigma Aldrich	E10521-10G
PTU	Sigma Aldrich	P7629-25G
Fluoromount G	Southern BioTech	0100-01
Low melt agarose	IBI Scientific	IB70051
Methylcellulose	Sigma Aldrich	M0387-100G
Paraformaldehyde	Sigma-Aldrich	158127-500G
UltraPure™ Distilled Water	Invitrogen	10977-015
Critical commercial assays		
Aval enzyme for st95 genotyping	Biolabs	R0152L
Experimental models: organisms/strains		
Danio rerio (zebrafish)	see Experimental model and subject details	N/A
Oligonucleotides		
St95 F primer	ACATAAGGCGTAGAGATTGGACG	Reference: Shiau et al. (2015) ⁶³
St95 R primer	GAAACATAGTGCGGTCCTCATCC	Reference: Shiau et al. (2015) ⁶³
GFP F primer	TATATCATGGCCGACAAGCA	N/A
GFP R primer	CTGGGTGGCTCAGGTAGTGG	N/A
DsRed F primer	TCCGAGGACGTCATCAAGGAGTTC	N/A
DsRed R primer	GGCGGGGTGCTTCACGTACAC	N/A

RESOURCE AVAILABILITY

Lead contact

Further information and requests for resources and reagents should be directed to and will be fulfilled by the lead contact, Celia Shiau (shiauce@unc.edu).

Materials availability

This study did not generate new unique reagents.

Data and code availability

The published article includes all data sets generated or analyzed during this study.

EXPERIMENTAL MODEL AND SUBJECT DETAILS

Zebrafish husbandry and lines

All fish used in this study were reared and maintained in the Zebrafish Aquaculture Core Facility at UNC Chapel Hill under 14-hr light / 10-hr dark cycle and 28°C and according to standard procedures. Fish used in this study were wild-type AB and TL lines; transgenic lines: Tg(*mpeg1*:GFP), Tg(*nbt*:DsRed), and Tg(*sm22 α -b*:GFP); and mutant line *irf8*^{st95}. Heterozygotes were in-crossed to obtain homozygous *irf8* mutants. Tg(*sm22 α -b*:GFP)(Seiler et al., 2010) fish were a kind gift of Dr. Michael Pack (University of Pennsylvania). Embryos were treated with 0.003% 1-phenyl-2-thiourea (Sigma-Aldrich) until 5 dpf to enhance optical clarity. Since zebrafish sex is determined on a polygenic basis and influenced by environmental factors, they are not definitively defined until reaching near adult stages at around 3-month postfertilization. Most analyses in this study took place prior to sex determination, while any study using adult stages, equal numbers of males and females were assigned for each experimental group. This study was carried out in accordance with the approval of UNC-Chapel Hill Institutional Animal Care and Use Committee (protocols 16–160 and 19–132).

METHOD DETAILS

Tissue preparation and immunostaining

Zebrafish were euthanized in a lethal dose of tricaine and decapitated. The entire gut was dissected (\geq 6 dpf), opened longitudinally (\geq 9 dpf), and cleaned with phosphate buffered saline (PBS) to remove gut contents. For imaging of endogenous fluorescent signal, the tissue was then oriented open-faced on a glass slide and mounted (Fluoromount G) with either the villar-ridge or muscle side nearest the objective for luminal or muscular analysis, respectively. The tissue was fixed with 4% PFA / PBS solution for 16 hr at 4°C. Following fixation, tissue was washed and permeabilized with 0.2 % triton X-100 in PBS (PBT) and blocked in PBT containing 5% normal goat serum (NGS). Primary antibodies were applied in fresh blocking buffer 16 - 72 hr at 4°C. Following primary antibody application, samples were washed in PBT and secondary antibodies applied for 1-3 hr at room temperature prior to mounting and imaging.

Quantification of gut macrophages and measurements of body/gut lengths

SL was quantified at time of sacrifice using a standard ruler. Gut length was measured *ex vivo* using coded software length measurement tools (ImageJ). Macrophages were quantified as discrete *mpeg1*:GFP+ cells using the counter tool (ImageJ). All counts were made in *ex vivo* extraction of whole gut at all stages to ensure an accurate count of only macrophages residing in the intestines and not those surrounding outside of the gut.

Classification of the MM ϕ occupation

MM ϕ occupation was determined by visual analysis of *mpeg1*:GFP+ cell bodies and projections occupying the muscularis externa relative to neural projections (*nbt*+ or acetylated tubulin) in order to determine discrete layer occupation. Occupation range was coded from beginning of signal (most proximal *mpeg1*:GFP+ projection) to end of signal (most distal *mpeg1*:GFP+ projection) from a single *mpeg1*:GFP+ cell body.

Larval intestinal transit and motility assessments

Fish were raised from *irf8*^{st95/+} heterozygous in-cross and put on a rotifer diet beginning at 5 dpf and grown to 10-11 dpf to a size of 5.5 mm SL prior to experimentation. The rotifer diet consists of about 50 rotifers/ml in 5 parts per thousand saltwater in a total volume of 400 ml fish water contained in a tank that is supplemented with 2 ml/L of RG Complete for feeding rotifers. Up to 10 dpf, the larval zebrafish is maintained at about 1000 rotifers per fish by either adding more rotifers or only replenishing the feed RG Complete and grown in static water, then moved to the recirculating zebrafish aquaculture system (Techniplast) starting at 10 dpf with 1 drip per second of water. They were fed *ad libitum* up to 10-11 dpf at which point food was withdrawn (timepoint 0) for the remainder of the time-course (Figure 6). Two independent experiments were conducted for each of the larval gut transit and motility assays in a blinded fashion and genotyping was performed only after data acquisition and analysis.

For the larval intestinal transit assessment, a longitudinal study was conducted to track the same individual larval zebrafish over time as gut contents were passed through the intestine. Color static images of the gut region in the living larval zebrafish embedded in 3% methyl cellulose were taken on a Leica S9i digital

stereoscope integrated with a 10 megapixels high quality color camera. Fish were kept separately in 24-well tissue culture dish in clean fish water during this time-course as they were individually taken out every 1-2 hours for a quick image of the gut region until all intestinal content was emptied. Gut content was calculated by using the ROI tool on ImageJ to conduct an area measurement of the gut content based on arbitrary units (A.U.) (see [Figure 6](#)). For the larval intestinal motility assessment, individuals were mounted in 0.75% low-melting agarose oriented on the sagittal plane. *In vivo* video recording of gut motility using bright-field microscopy was captured at 1 frame per second for 5 minutes using an automated acquisition software on a Leica M165 FC stereomicroscope with a high-speed monochrome sCMOS camera (DFC9000 GT). Videos of the living larval zebrafish were captured within the first hour the zebrafish were removed from food and placed into clean fish water (see [Videos S1](#), [S2](#), and [S3](#)). Intestinal motility for each individual was measured by counting the number of peristaltic waves (anterograde and retrograde along the gut) and rectal contractions that occurred (see [Figure 6](#)) using playback video analysis.

Adult gut transit assessment

Fish were raised from *irfb^{st95/+}* heterozygous incross and grown to 1.0-1.5 cm SL stage prior to experimentation. Fish were allowed to feed ad libitum prior to food 24-hour food withdrawal (timepoint 1), allowed to feed ad libitum for another 24 hours (timepoint 2) and withdrawn again for another 24 hours (timepoint 3). At each timepoint, fish were collected for sacrifice and the gut carefully resected so as not to disturb intestinal contents and imaged with a low magnification stereoscope (described below). Gut content was calculated by measuring the sum of gut length occupied by contents relative to total gut length. Adult zebrafish were co-housed and fed twice daily using conventional dry food diet (GEMMA Micro 300) providing an amount estimated to account for 1-5% of daily body weight for all fish in the tank until the 24-hour food withdraw timepoint. Fish were processed and split three-ways for three discrete timepoint analyses. The first subset of the adults was used for endpoint gut content analysis at the 24-hour food withdraw timepoint, while the remaining fish were given feeding for another 24 hours (2 meals of GEMM Micro 300). A second subset was used for the 24-hour feed timepoint analysis to assess food intake after 24 hours of feeding. The final remaining cohort of fish was processed at the 48-hour food withdraw timepoint after 24 hours of feeding to assess gut content. Experiments were conducted in a blinded fashion and genotyping of all fish was performed after data acquisition and analysis. Two independent experiments as described were conducted.

Vibratome sectioning

Samples were fixed overnight in 4% PFA at 4°C and washed with PBT prior to embedding and sectioning via vibratome in 1.5% low melt agarose. Acquired 200-400 µm sections were subjected to antibody immunolabeling as described above.

Imaging and Image Analysis

Confocal imaging was performed on a Nikon A1R+ hybrid galvano and resonant scanning confocal system equipped with an ultra-high speed A1-SHR scan head and controller. Images were obtained using an apochromat lambda 40x water immersion objective (NA 1.15) or a plan apochromat lambda 20x objective (NA 0.75). Z-steps 0.5 – 5µm were taken at 20x and 40x. Nyquist sampling was employed where noted. NIS Elements AR (Nikon) visualization software was used. Confocal micrographs were also analyzed with ImageJ software and Imaris Viewer.

QUANTIFICATION AND STATISTICAL ANALYSIS

Standard error of the mean (S.E.M.) is shown unless otherwise noted. p-values are included in figure legends. Unpaired T test was used to determine significance between two groups. One-way ANOVA was used to determine significance between three groups or more. Statistical analyses were performed using GraphPad Prism software (GraphPad, San Diego, CA, USA).

ADDITIONAL RESOURCES

See [Supplemental information](#).